Faculty of Mathematical, Physical and Natural Sciences
Department of Environmental Sciences
University of Milano-Bicocca

Carbon dioxide exchange of an alpine grassland: integration of eddy covariance, proximal sensing and models

PhD Dissertation
Cycle XXIII

Candidate:
Dr. Marta Galvagno

Supervisor: Dr. R. Colombo

Advisor: Dr. G. Manca

Coordinator: Prof. M. Vighi

July 2011

Acknowledgements

I would like to thank first of all my supervisor, Roberto Colombo who made possible this work and for scientific insights during the research activity. I'm really grateful to Mirco Migliavacca for invaluable scientific, technical and moral support and guidance, and to Edoardo Cremonese for daily relevant discussions, the precious help and personal training. I would like to thank Giovanni Manca for its essential technical and theoretical support in eddy covariance measurements and for introducing me to instrumental set-up and data processing. A special thank to Micol Rossini for advices on spectral measurements and for all the important insights and comments in these three years. I would like to thank Umberto Morra di Cella for constant useful discussions and fundamental technical support. Many thanks to all other members of my group: Paolo Pogliotti and Fabrizio Diotri, especially for Linux and Latex tricks and Gianluca Filippa for useful scientific exchanges. Thanks to the LTDA group, especially to Sergio Cogliati, Lorenzo Busetto, Cinzia Panigada for support and interesting talks. I would like to thank Georg Wohlfahrt for fruitful discussions in Innsbruck and helpful suggestions. Acknowledgements to Consolata Siniscalco for advices on phenological topics, and to Emiliano Pari, Martina Petey, Sara d'Alessandro and Emily Solly for phenology field campaigns. I further acknowledge the Torgnon community in hosting this activity. Thanks to my family for constant support and finally thanks to Tommaso, who started the PhD course with me and every day of my life reminds me of the most important things.

Contents

Abstract

The terrestrial biosphere represents a large pool of carbon, whose cycle is governed by the opposed processes of CO_2 uptake (photosynthesis) and release (respiration) from and to the atmosphere. Considering the role of carbon dioxide in the observed global warming, monitoring, understanding and modeling carbon exchange of ecosystems is a critical issue in climate change researches. Moreover because of the multiple implications of vegetation structure dynamics on ecosystem carbon fluxes, monitoring and modeling plant phenology is also of increasing scientific interest.

Among terrestrial ecosystem grasslands cover almost 40% of ice-free land surface, nevertheless their role as sources/sinks of atmospheric CO_2 is not well clarified.

In this study the eddy covariance method was used to assess CO_2 exchange at an high elevation unmanaged grassland in the North-Western Italian Alps (Aosta Valley - Torgnon), during three years (2008-2010) of measurements and to evaluate how environmental factors affect photosynthetic processes.

The seasonal and inter-annual course of net ecosystem CO_2 exchange (NEE), ecosystem respiration (Reco), gross primary production (GPP) and the main meteorological variables was analysed. The three growing seasons had a similar seasonal dynamic, characterised by a fast rise of photosynthetic activity after snow-melt followed by a gradual autumnal decline. Regarding the meteorological variables, only precipitation, soil water content and snow depth differed markedly among two of the studied years (2009-2010) compared to other factors which showed only small differences in restricted time-periods.

To better interpret how weather variables modulate ecosystem processes at multiple time-scales (day, week, month, year), a quantitative analysis was performed

applying wavelet coherence between time-series of GPP and time-series of different meteorological factors (air and soil temperature, soil water content and photosynthetically active radiation).

Eddy covariance and meteorological data were combined with proximal sensing measurements to identify links between optical indices, canopy development and fluxes. In particular a colour index derived from continuous digital imagery (i.e. Greenness Index, (GI), based on RGB channels) and indices derived from an HyperSpectral System (Hyperspectral Irradiometer, HSI) were used as input to simulate GPP, based on a light use efficiency (LUE) model. Results showed that a LUE model driven by optical indices and meteorological variables is able to describe the GPP trend in the two years of study. In particular the use of different model formulations provided insights on the role of the main meteorological factors controlling grassland photosynthesis. The comprehension of these relationships at stand level is essential for extrapolating such information at different spatial scales.

List of Figures

List of Tables

1 Introduction

1.1 Framework

Terrestrial ecosystems and the climate system are closely coupled, particularly by cycling of carbon between vegetation, soils and the atmosphere. (*Cao and Woodward*, 1998). Photosynthesis is the mechanism by which terrestrial ecosystems gain carbon dioxide (CO_2) from the atmosphere, contributing in this way to the terrestrial annual uptake of 120 GtC per year (*Solomon*, 2007). A fraction of carbon fixed by gross primary production (GPP) of vegetated terrestrial surface is released via ecosystem respiration (Reco) back to the atmosphere. The small imbalance between these two large processes is termed net ecosystem exchange (NEE) and shows a strong diurnal, seasonal and annual variability (*Valentini et al.*, 2000).

Human activities make a significant contribution to the global carbon cycle (e.g. fossil fuels combustion, cement production, land use changes, ...) and cause atmospheric CO_2 concentration to increase exponentially since the beginning of the Industrial Revolution (*Chapin et al.*, 2002). Since CO_2 is one of the major responsible of the observed global warming (*Solomon*, 2007), particular attention of the scientific community has been recently addressed to assess the role of different ecosystems on the global carbon and water cycles (*Baldocchi*, 2008) and how component fluxes are controlled by biotic, abiotic and management factors (*Wohlfahrt et al.*, 2008a). In this framework a better understanding of the processes that regulate the interactions between environment and organisms, at multiple spatial and temporal scale, is the basis to increase confidence in predictions of ecosystem responses and feedbacks to recent and future global changes.

In the past years substantial attention has been addressed to the carbon seques-

tration of forests (*Valentini et al.*, 2000; *Misson et al.*, 2007), while data on carbon exchanges of non-forest ecosystems and in particular on natural (or semi natural) grasslands remained generally poor represented (*Cernusca et al.*, 2008). As grasslands represent about 40% of the global terrestrial ice-free surface (*White et al.*, 2000) an increasing number of research are currently focusing on the carbon exchange related processes of grassland ecosystems (e.g. *Flanagan et al.* 2002; *Xu and Baldocchi* 2004; *Soussana et al.* 2007). In particular the assessment of carbon exchange in mountain grasslands has recently received more attention (*Wohlfahrt et al.*, 2003; *Rogiers et al.*, 2005; *Wohlfahrt et al.*, 2008a; *Zeeman et al.*, 2010), but a complete understanding of ecosystem processes in high elevation alpine sites is still lacking.

Moreover, physiological activities of plants are strictly related to their phenology (i.e. the timing of recurrent biological events and the causes of their temporal change, *Lieth* 1974). As a consequence, since the state of canopy development has a great control on spatial and temporal patterns of the vegetation/atmosphere exchange of carbon and water (*Richardson et al.*, 2007b), monitoring and modeling vegetation phenological cycle became a key issue in the analysis of the interactions between climate and ecosystems (*Baldocchi and Wilson*, 2001).

Mountain regions are expected to be particularly influenced by future climate change with increasing temperature, change in precipitation patterns and duration of snow cover. Environmental drivers that affect ecosystem processes are numerous and occur over a wide range of temporal and spatial scales. As a consequence the evaluation of the impact of climate change on ecosystems requires long-term series of data and the integration of a variety of observations. The wide distribution of alpine ecosystems at all latitudes makes these cold environments important resources for monitoring and understanding climate change effects on a global scale and long-term alpine research sites represent invaluable reference points for global change researches. (*Körner*, 2003).

1.1.1 Current approaches in carbon cycle studies

1.1.1.1 Micrometeorological flux measurements

Carbon dioxide exchange between the ecosystem and the atmosphere can be reliably quantified using the eddy covariance method (*Baldocchi et al.*, 1988; *Aubinet et al.*, 2000; *Baldocchi*, 2003). Eddy covariance is a micrometeorological technique that assesses gas exchanges across the biosphere/atmosphere interface by measuring the covariance between vertical wind velocity and gas mixing ratio. This technique provides accurate and continuous measurements of CO_2 net ecosystem exchange (NEE) at an appropriate (ecosystem) spatial scale. From these measurements, the other flux components of the carbon cycle, GPP and Reco can be derived through modeling approaches (*Reichstein et al.*, 2005; *Wohlfahrt et al.*, 2005b,a; *Lasslop et al.*, 2010). A worldwide network of micrometeorological stations (FluxNet) has been recently established (*Baldocchi et al.*, 2001a) in order to evaluate carbon exchange (water vapour and energy) dynamics in different ecosystems and create an integrated database for synthesis and modeling. A wider description of the method is given in chapter 2.

1.1.1.2 Remote sensing

A current interest of the scientific community is focused on the creation of a consistent global dataset of primary production estimates (*Heinsch et al.*, 2006). Eddy covariance measurements have greatly improved our understanding of carbon cycle over the past decades but tower-based estimates of primary production are restricted to spatially discrete observations. Remote Sensing techniques can be used to provide spatially-distributed, estimates of carbon cycle related processes. Current strategies based on optical Remote Sensing mainly rely on spectral reflectance properties of the vegetated terrestrial surface. Data offered by several Earth observing systems provide informations on structural or biochemical vegetation properties, that can be used to derive estimates of vegetation structure, phenology and potential photosynthetic rates. Moreover photosynthesis, expressed as Gross Primary Production, can be estimated by means of Remote Sensing based GPP models (chapter 2).

1.1.1.3 Monitoring phenology

Phenology is defined as the study of the timing of periodic events in organism life-cycle and the causes of their temporal change (*Lieth*, 1974). Several aspects of vegetation phenology are considered important indicator of biological impacts of climate change (*Menzel et al.*, 2006; *Solomon*, 2007). Inter-annual variations in the dates of bud-burst, leaf unfolding, leaf yellowing and growing season length are correlated with fluctuations in meteorological variables. Furthermore, phenology has multiple implications on the ecosystem carbon, water and energy fluxes. For these reasons, different methods to observe and model vegetation phenology and to quantify the effect that phenological changes could have on carbon sequestration have been developed. Phenological events can be observed on ground or extracted from remotely sensed data. Traditional field observations of specific phases of plant development can provide detailed information, especially to characterize species specific phenological response to inter-annual changes in temperature. Nevertheless this kind of data is affected by a poor temporal and spatial resolution and by the subjectivity of the observer. In this context, remote sensing data can allow the estimation of phenological variables from local to global scale. In the last two decades many studies have demonstrated the potential of multi-temporal satellite remote sensing data to characterize seasonal patterns of vegetation dynamics at a medium or coarse spatial and temporal resolution (*White et al.*, 2009). Recent studies (*Sims et al.*, 2006) highlighted the potential of proximal remote sensing methods to quantify seasonal patterns of vegetation development at ecosystem level with high temporal resolution. In the last years, the use of repeated digital images collected by commercial webcam has been demonstrated useful for phenological monitoring because it allows the collection of automated observations of canopy structure at high temporal frequency in a very simple and low cost way (*Richardson et al.*, 2007b, 2009a; *Migliavacca et al.*, 2011a). An important step towards the standardisation of this approach is represented by the north-american webcam network, PhenoCam, that has been initiated in order to provide automated and continued proximal sensing of canopy phenology across different ecosystems and climate zones. Collected data also contribute to efforts in which remote sensing is used to scale up intensively monitored sites to more extensive spatial domains (http://klima.sr.unh.edu/index.html). Moreover informa-

tion on vegetation development and functioning, at the scale of ecosystem, can be obtained with automatic tower-based spectral reflectance measurements (*Hilker et al.*, 2008) through the evaluation of indices related to the vegetation greenness (e.g. NDVI, *Rouse et al.* 1974, MTCI, *Dash and Curran* 2004). The simultaneous acquisition of vegetation indices and eddy covariance measurements is a valuable approach to a better understanding of the relation between phenology, carbon sequestration and optical signals. The use of remote as opposed to proximal spectral sensors for photosynthesis estimation may become a powerful tool in better understanding the spatio-temporal variations of productivity on a broader scale and scale up local carbon estimates to regional and global level.

1.2 Motivation and Objectives

This study aims at measuring CO_2 exchange dynamics and canopy development of an unmanaged subalpine grassland, by means of eddy covariance measurements integrated with proximal sensing observations and models.

This research is motivated by the recent attention of the scientific community on the role of diverse ecosystems on global carbon cycle and on the understanding of their feedbacks to recent and future climate changes.

The research is carried out in Aosta Valley, a small mountain region of Northwest Italy, characterized by an alpine climate (i.e. cold winter, mild summer, long snow season). Managed, grazed, abandoned and unmanaged grasslands cover an high percentage (30-40%) of the regional land surface, however no studies have never been accomplished on carbon exchange dynamics of these ecosystems at the time of this study and are quite rare in the European Alps.

Specific objectives concern:

1. the investigation of the magnitude, direction and variability of NEE and its components GPP and Reco, during three years of eddy covariance measurements in a poorly investigated ecosystem;

2. the use of a digital camera as a proximal sensing approach to monitor canopy phenology in a continuous and automated way in order to evaluate the relationship between ecosystem function and structure;

3. the assessment of the role of environmental factors on carbon fluxes at multiple temporal scales;

4. the application of remote sensing based models to evaluate the use of optical vegetation indices in the estimation of seasonal GPP dynamics.

Structure of the dissertation

- The dissertation begins in chapter 2: some theoretical topics on plant physiology and on the techniques used in this study are briefly described to introduce issues discussed in the specific sections.

- In chapter 3 general informations on the study site are given, followed by the description of instruments installation and set-up. The methods for eddy covariance and digital camera data processing are then described in detail.
- In chapter 4 results of this research are presented, organised in three major parts: the assessment of the carbon balance dynamics and phenology of the grassland, the evaluation of the timing of environmental influences over carbon exchange and the modeling of GPP at ecosystem level on the basis of optical vegetation indices.
- In chapter 5 results presented in chapter 4, are discussed.

This work was supported by the PhenoALP project, an Interreg project co-funded by the European Regional Development Fund, under the operational program for territorial cooperation Italy-France (ALCOTRA) 2007-2013

PhenoAlp project: an integrated approach to study phenology in the Alps

PhenoAlp[1] is an Interreg project, co-founded by the European Regional Development Found, under the operational program for territorial cooperation Italy-France (ALCOTRA) 2007-2013.
The project aims at better understanding of phonological changes in the Alps.
Project leader is the Environmental Protection Agency of the AostaValley (ARPA Valle d'Aosta, Italy).

The main research goals of this project are:

- To implement a network of observations in the involved territories (Valle d' Aosta and Savoies);
- To define a common strategy of observation and common protocols;
- To involve local communities and schools in observing phenology, with the aim of increasing people's awareness on the issue of climate change.

The project is organised in seven actions:

1. Pheno-Plant deals with alpine vegetation phenological cycle and one of its aim is to develop climate change indicators on the basis of plant phenology.
Regarding alpine grassland phenology a new protocol for field observation was developed based on most common growth forms of these ecosystems;
2. Pheno-Detect aim is to track alpine vegetation phenology using satellite data and webcam images;
3. Pheno-Flux aims at assessing the relationship between plant growing season length and ecosystem productivity, measured as carbon dioxide (CO_2) exchange of the ecosystem.
Two sites are monitored in the framework of PhenoAlp: an alpine grassland and a larch forest (Torgnon, 2160 m asl);
4. with Pheno-Zoo a wide range of animal taxa is considered to detect which are the most suited for phenological monitoring in the Alps;
5. The aim of Meteo-Reseasu is to create a network of meteorological stations in the phenological observation sites;
6. Inter-Pheno concerns the integrated evaluation of the effects of climate change on plant and animal phenology;
7. Pheno-Form aims to involve local communities (e.g. schools naturalistic guides, forest rangers...) in phenological observation activities as a way to increase the public awareness on the issue of climate change in the Alps.

PhenoAlp project started in 2009 and will last until 2012.

1 - http://www.phenoalp.eu/

2 SCIENTIFIC BACKGROUND

2.1 Ecosystem Carbon Balance

By definition, the carbon balance of an ecosystem at any point in time is the difference between its carbon gains and losses (*Heimann and Reichstein*, 2008). Carbon enters the ecosystem through photosynthesis, the processes by which autotrophs (plants and photosynthetic bacteria) produce their own organic compounds; most of this carbon returns in the atmosphere by autotrophic and heterotrophic (animals, fungi and microorgnanism) respiration (others losses of carbon could be as volatile organic compounds, methane or dissolved carbon).

The metabolic processes of organisms hence constitute the engine that drives the global carbon cycle on time scales of seconds (e.g., photosynthetic rates, stomatal conductanece) to centuries (large-scale climatic changes) (*Chapin et al.*, 2002). The majors pools of carbon are: the atmosphere, oceans, vegetation and soil, sediments and rocks. Within these, while the atmosphere, mainly composed of CO_2, is the smallest (but most dynamic) pool, the terrestrial biosphere is the largest biological reservoir of carbon (*Chapin et al.*, 2002).

Particular attention of ecosystem science studies is on the the interactions between organisms and the environment and on the resulting feedbacks. For convention, a positive feedbacks is when an interaction trigger to an increase of the environmental change, and a negative feedbacks is when interactions reduce changes.

A better knowledge of controls over the interaction and feedbacks between terrestrial ecosystem processes and the atmosphere is important to understand how the Earth System will respond to current trends of increasing temperature and atmospheric CO_2.

Following some topics on photosynthesis and respiration are briefly described to introduce issues discussed in the specific sections.

2.1.1 Photosynthesis

Photosynthesis is the physiological process by which plants (and other autotrophs) synthesize complex molecules as carbohydrates and produce oxygen (O_2), starting from simple molecules as carbon dioxide (CO_2) and water and using light as source of energy. The description of photosynthesis reactions presented in this section is mainly based on the textbook of *Taiz and Zeiger* (2010). The overall reaction of photosynthesis can be summarized as:

$$CO_2 + H_2O \xrightarrow{\text{light}} (CH_2O) + O_2 \tag{2.1}$$

The wide and complex series of photosynthesis reactions that ends with the reduction of CO_2 to organic compound, is traditionally divided into two parts: the reactions that require the utilization of light and the reactions of carbon fixation (light reactions and carbon reactions, respectively, in figure 2.1) .

1. The light-dependent reactions are the first stage of photosynthesis and involve photosynthetic pigments, chlorophylls and carotenoids to capture and store energy from sunlight. During this process, light energy is converted into chemical energy, in the form of molecules of ATP and NADPH and water is oxidized with production of O_2. Solar radiation active in photochemical processes (Photosynthetically Active Radiation, PAR) includes wavelengths of visible region of the solar spectrum, approximately between 400 and 700 nm. In higher plants, light-dependent reactions take place on the internal membranes (thylakoid) inside the photosynthetic organelles, the chloroplasts, where specialized molecular complexes (photosystems) catalyze the light-dependent reactions through a series of redox reactions, called on the whole, electron transport chain (ETC).

2. Strictly coupled with the production of energy in the form of ATP and NADPH is the next process of photosynthesis, *Calvin cycle*, during which CO_2 is fixed

into organic compounds and reduced into carbohydrates. This step of photosynthesis is finely regulated by different cell enzymes in order that energy and all the intermediates needed for carbon fixation are available and that the mechanism is turned off in the dark. The chemical reactions involved, that take place in the stroma of the chloroplast outside of the internal membranes, can be considered as divided into three phases collectively: carboxylation, reduction reactions, and regeneration. Temporal and spatial differences in the metabolic path of this process exist among species and will be briefly described hereinafter, nevertheless the basic mechanism is the same.

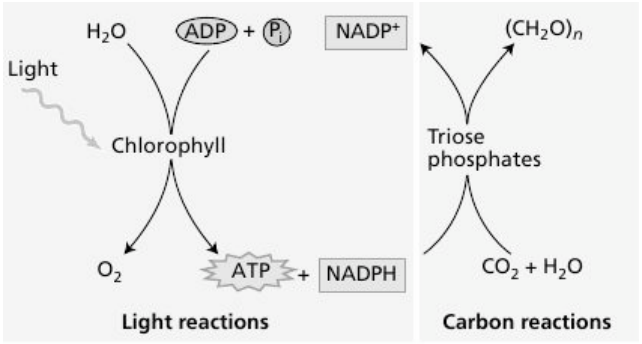

Figure 2.1: *Light reactions and carbon reactions of photosynthesis (from Taiz and Zeiger (2010) modified).*

In plants with a C_3 metabolism,

- carbon dioxide coming from the atmosphere is enzymatically attached to a 5-carbon acceptor molecule, the ribulose-1,5-bisphosphate (RuBP), by the enzyme RuBP carboxylase/oxygenase (Rubisco); two of 3-carbon intermediates (3-phosphoglyceric acid, PGA) are generated;
- the molecules of PGA are reduced to form molecules of the carbohydrate glyceraldehyde 3-phosphate (G3P), a triose phosphate. This reaction uses the energy from ATP and NADPH generated photochemically. A portion of the triose phosphates generated is converted into storage forms of energy and carbon: sucrose and amide, while a part is used in the reaction of regeneration;
- in order for the process of carbon fixation to continue (and so new CO_2

molecules entering the chloroplasts to be continuously fixed), the cycle closes with the regeneration of the first acceptor RuBP, from molecules of G3P.

The enzyme Rubisco has double activity of carboxylase/oxygenase, that is it has an alternatively affinity for CO_2 or O_2 within the same active site, depending on the relative cell concentrations of the two gases. In the case that oxygenation of the first acceptor of the cycle(RuBP) take place, carbon dioxide is released from the cell, rather than fixed, and photosynthetic efficiency is reduced; This process is called photorespiration. In optimal environmental conditions, CO_2 concentration in the cell is higher than O_2 and Rubisco shows a greater affinity for CO_2 molecules. As temperature rises, CO_2 concentration in the cell declines quicker than O_2, and photorespiration prevails on photosynthesis. In some species, commonly typical of arid and hot environments, different paths in the carbon fixation reactions protect the plant from an excessive photorespiration,

- in C_4 species, the location of CO_2 absorption and carbon-fixation is spatially split. Carbon dioxide is temporary fixed to form a 4-carbon intermediate and transferred into particular cells (bundle sheath) where it is released and enters in the calvin cycle; the possibility to highly concentrate the CO_2 into these cells favours photosynthesis against photorespiration;

- in CAM (Crassulacean Acid Metabolism) species, the location of CO_2 absorption and carbon-fixation is temporally split. CAM plants open stomata during the night, when air temperature is lower and relative humidity is higher; CO_2 absorbed is accumulated into the vacuole of the cell. During the day, when stomata are closed, CO_2 in the form of 4-carbon intermediate is transferred in the chloroplast end enters the Calvin cycle.

In summary, leaf photosynthesis depends on the capacity of light utilization, the diffusion of CO_2 from the atmosphere to the site of carboxilation, the formation of

assimilates and the regeneration of photosynthetic substrates. These steps in turn depend on the tissue developmental stage, the availability of water and nutrients and environmental factors, which finally influence the overall plant (or canopy) photosynthetic rate.

2.1.2 Respiration

Plant respiration is the process by which energy stored in the form of carbohydrates trough photosynthesis is released and used for maintenance and development of metabolic activities. During respiration carbon compounds are oxidized with the liberation of CO_2 and the production of ATP. The general reaction of respiration can be summarized as:

$$(CH_2O) + O_2 \rightarrow CO_2 + H_2O + \text{energy} \tag{2.2}$$

Respiration reactions are divided in three main steps: glycolysis, citric acid cycle, and oxidative phosphorylation.

- During glycolysis, in the cytoplasm of the cell, a 6-carbon molecule is broken into pyruvic acid, a 3-carbon molecule, with production of a small amount of energy (ATP) and reducing power (NADH);
- pyruvate is subsequently oxidized trough the citric acid cycle that takes place in the matrix of the mitochondrion, in the process molecules of NADH and FADH2 are produced;
- during the oxidative phosphorylation process electrons are transferred along an electron transport chain, in the inner of the two mitochondrial membranes. This system transfers electrons from NADH to oxygen, releasing a large amount of free energy in the form of ATP.

At the ecosystem scale, respiration consists of both plant respiration and heterotrophic respiration from non-photosynthetic organisms (microorganisms and animals). Moreover ecosystem respiration can be partitioned into aboveground respiration and belowground, i.e. soil, respiration. The latter constitutes one of the major flux of

carbon between terrestrial ecosystems and the atmosphere (*Bahn et al.*, 2008) and is composed by microbial decomposition of soil organic matter and by plant belowground (root) respiration.

Both respiration components (autotrophic and heterotrophic) are strictly related to the respective substrate availability (photosynthates, litter and soil organic matter), providing a direct link between respiration and photosynthesis (*Chapin et al.*, 2002; *Wohlfahrt et al.*, 2008a; *Migliavacca et al.*, 2011b).

2.1.3 Definition of ecosystem carbon exchange terms

When the processes of carbon gain and loss are considered at the ecosystem scale the following terms are used:

Gross Primary Production (GPP): is the gross uptake of carbon by photosynthesis of all plants of the ecosystem

Ecosystem Respiration (Reco): is the combined autotrophic respiration by plants (Ra), and heterotrophic respiration by animals and microorganisms (Rh).

Net Ecosystem Exchange (NEE): is the net exchange of CO_2 between the ecosystem and the atmosphere, resulting from the balance between the assimilatory and respiratory processes.

NEE is the small net difference between two larger fluxes: GPP and Reco. Under favourable conditions, the net ecosystem flux is dominated by photosynthesis during daytime, and by respiration at night and, at temperate and high latitude (or in deciduous ecosystems) in non-vegetative periods. In detail, during the growing season (the period when vegetation is photosynthetically active), NEE is negative indicating that photosynthesis exceeds respiration, while during period of inactivity of vegetation, photosynthesis is low or absent, and NEE has positive values indicating net loss of carbon due to respiratory processes (mainly heterotrophic).

As ecosystems continuously absorb and release CO_2 by and to the atmosphere, the analysis and modelling of the CO_2 quantities described above are used to define whether a system is a net source or sink of carbon at different temporal scales and to understand the effects that biological and physical controls have on CO_2 absorption, sequestration, and release activities.

2.1.4 Environmental controls

In natural condition, plants continuously respond to different environmental drivers that can in turn regulate their metabolic activities (mainly photosynthesis and respiration). When one of these abiotic factors assumes values out of the optimal range for plant life and as a consequence it exerts a disadvantageous influence on the whole plant functioning, it becomes a stress factor.

Environmental factors that can limit or stress vegetation are numerous and have different influences on different metabolic paths; among these, light, temperature, water availability, nutrient availability and atmospheric gas concentration generally exert the greatest role. Considering the alpine and subalpine vegetation, winter snow cover depth and duration are of great importance; the presence of snow on ground fully limits the length of the growing season in herbaceous species and has a great influence on photosynthetic activity for both deciduous and evergreen tree species (*Monson et al.*, 2005). Despite its adverse effects, snow has an important protective role for example from exposure to low air and soil temperature extremes and from winter dessication (*Körner*, 2003). Furthermore, during spring recovery, when others environmental conditions are favourable for plant development (temperature, photoperiod..) snow melt is also a great source of water and nutrients accumulated over the winter.

Several studies are focused to understand the role of environmental factors on photosynthesis and respiration, and on the whole carbon exchange of ecosystems. Nevertheless, because this investigation involves the consideration of complex mechanisms as the functioning of photosynthetic light-harvesting system, carbon fixation and allocation, substrate availability for respiration, biotic interactions...the distinction of the role of a single driver, is often complex. In particular, complications arise because of several controlling mechanisms that interact over multiple temporal scales from second to years (*Stoy et al.*, 2009), and act on different and complex biological processes (photosynthesis, autotrophic and heterotrophic respiration..) (*Vargas et al.*, 2011). Fast changes in sunlight influence short-term (less than 1 h) variations in photosynthesis, stomatal conductance, and respiration. Diel rhythms in PAR, air and soil temperature lead the daily carbon and water exchanges. At weekly scale changes in weather and precipitation pulses induce fluctuations in photosyn-

thesis and respiration. On monthly to seasonal times scales, changes in phenology, photoperiod, soil water balance and temperature influence the ecosystem processes. Climatic changes act on inter-annual, switching the timing of phenological events (*Baldocchi et al.*, 2001b).

2.2 Eddy Covariance method

In this section a brief introduction to the method employed to evaluate gas exchange of the ecosystem, i. e. the eddy covariance technique, is given. For a more complete and detailed review of eddy covariance theory, refer to the wide available literature (e.g., *Baldocchi et al.* 1988; *Goulden et al.* 1996; *Aubinet et al.* 2000; *Massman and Lee* 2002; *Baldocchi* 2003; *Foken* 2008) The eddy covariance technique is a micrometeorological method used to evaluate gas exchange across the interface between the atmosphere and the biosphere by measuring the covariance between vertical wind velocity and gas mixing ratio (*Baldocchi et al.*, 1988).

During past decades the eddy covariance method has emerged as one of the most direct and reliable way to measure fluxes of heat, water, CO_2 and other trace gases in different ecosystems. It is considered a suitable method for plant physiology studies at the whole-ecosystem scale and for the analysis of the role of environmental drivers on ecosystem functioning. (*Baldocchi*, 2003).

In the past years, regional, national and international networks (e.g., FluxNet, AmeriFlux, ICOS, CarboEurope...), are born and collect flux data measured with eddy covariance coming from different ecosystems. Flux networks allow important activities as data synthesis and modelling, intercomparison between sites, evaluation of ecological topics and are involved to unify the procedures of eddy covariance flux calculations. Currently, over 500 eddy covariance sites are present worldwide (http://www.fluxnet.ornl.gov/).

Despite other methods exist, as cuvette and chambers, to measure carbon dioxide exchange of vegetation, eddy covariance presents remarkable advantages, overall on temporal and spatial basis: the system can perform direct estimates of the net exchange of CO_2 at a very high temporal resolution and permits the integration over a wide range of time scales from hours to years; it is a scale-appropriate method

because it considers the whole ecosystem and the measured flux represents the integrated value of the fluxes between the atmosphere and the ecosystem of an area from few meters to several kilometres; the instrumentation employed does not alter the environment analysed (*Baldocchi*, 2003).

Nevertheless eddy covariance method requires some specific assumptions to be applied correctly: the terrain is flat and uniform, measurements at a point represent an upwind area, flux is fully turbulent, air density fluctuations, flow divergence are negligible, the environmental conditions are steady and the vegetation type under study extends uniform upwind for a wide area. The non-complete respect of these assumptions and/or different kind of instrumental problems introduce errors, moreover many of the eddy covariance measurements sites are on undulating or gently sloping terrain, as this is where native vegetation exists (*Baldocchi et al.*, 2001a). Despite the disadvantages, a number of standardised procedures applied at different steps of the workflow of eddy covariance measurements serve to minimize or avoid errors (*Burba and Anderson*, 2010).

2.2.1 Eddy covariance theory

Eddy covariance assesses the turbulent fluxes in the lowest part of the atmosphere, i.e. within the planet boundary layer (PBL), at the interface between the biosphere and the atmosphere. PBL contains turbulent motions of upward and downward moving air called eddies, each characterised by a specific temperature, concentration of water vapour and gases such as CO_2. The eddy covariance instrumentation samples these motions to determine the difference between the amount of mass and energy that move downwards to the biosphere and upwards to the atmosphere, i.e. the net flux. (figure 2.2).

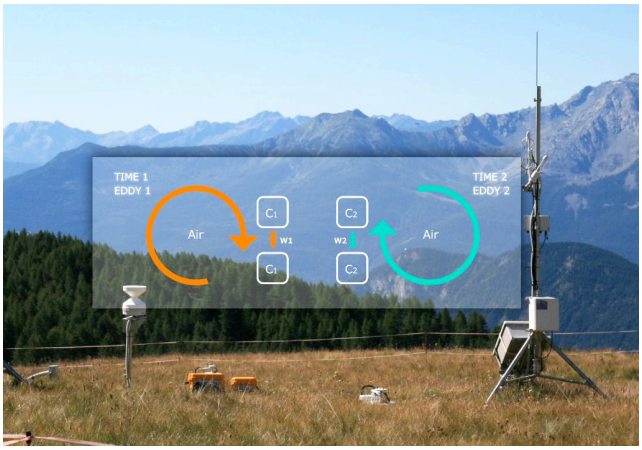

Figure 2.2: *Exemplification of eddy flux at a single point (from Burba and Anderson (2010) modified). At a given instant (time 1), eddy number 1 moves air parcel c1 downward with the speed w1. At the next instant (time 2) at the same point, eddy number 2 moves air parcel c2 upward with speed w2. Each air parcel has its own characteristics, such as gas concentration, temperature,humidity, etc. the eddy covariance samples how many molecules of gas go down to the biosphere with downward wind at time 1 and how many go up to the atmosphere with upward wind in time 2.*

In mathematical terms eddy flux is computed as the covariance between the instantaneous deviation in vertical wind speed (w') from its mean value (w) and the instantaneous deviation in gas mixing ratio (c'), from its mean value (c) and multiplied by mean air density; the vertical flux can be expressed by the following general equation (*Baldocchi*, 2003):

$$F = \overline{\rho_a}\ \overline{w'c'} \tag{2.3}$$

where overbar denotes temporal averaging (e.g. half-hour or hour), the prime denotes the deviation from the mean, ρ_a, the air density, w and c vertical wind speed and gas concentration respectively. Behind this final equation of flux, several mathematical computations (including Reynolds decomposition) and assumptions (air density fluctuations, divergence/convergence of turbulence flux are considered negligible) are involved (see *Burba and Anderson* 2010).

When the focus of the study is to assess the carbon exchange of ecosystem the measured gas is CO_2 and the turbulent measured flux coincides with term NEE that represents the net difference between the photosynthetic CO_2 assimilation by plants

and respiratory CO_2 release by both autotrophs and heterotrophs. For convention when the net flux is towards the vegetation, indicating net uptake of CO_2 by plants, NEE has negative sign, when the net flux is away from the surface, indicating release to the atmosphere, NEE has positive sign.

The net CO_2 flux can also be expressed as:

$$-NEE = GPP - Reco \tag{2.4}$$

As eddy covariance system computes the net flux of CO_2, the other components of the carbon cycle, i.e. GPP and Reco, could be derived trough modelling techniques. At present different flux partitioning approach exist (*Reichstein et al.*, 2005; *Wohlfahrt et al.*, 2005b,a) and will be described in the Matherials and Methods chapter (3).

2.2.2 Eddy covariance instrumentation

Common eddy covariance instrumentation is composed by a 3-dimensional (3-D) sonic anemometer for the measurement of wind speed in the three components (*w, u, v*) and an infra-red gas-analyser (IRGA) to evaluate atmospheric mixing ratios of CO_2 and H_2O (or another gas of interest). Instruments are mounted on a tower above the vegetation, at an height that depends on site characteristics (height of the vegetation, extent of the fetch, range of wind velocity and frequency response of the instruments). The turbulent up and down motions occur in part at very small temporal scales and in part at larger ones, for this reason eddy covariance requires sophisticated instrumentation to capture these fluctuations. In the last years several instrument models to perform measurements with very high frequencies such as 10 or 20 Hz have been developed, and are employed worldwide. An example of eddy covariance typical configuration is presented in figure 2.3.

While differences in the main functioning of 3-D sonic anemometers are not substantial, two different functional modalities exist for IRGA: *closed-path* system and *open-path* system. In closed-path systems air is actively pumped to the sample cell through a tube, while open-path gas-analyser assesses "*in situ*" free air. Both have advantages and disadvantages, and are generally more or less suitable to different

Figure 2.3: *Example of an Eddy Covariance installation, composed by a 3-D sonic anemometer (CSAT3, Campbell Scientific, Inc.) and an open-path IRGA (LI-7500, LI-COR , Inc., Lincoln, NE, USA)*

environmental conditions.

Open-path sensors require low power supply, don't have pump and tube and are suitable for harsh environments, on the other hand, they suffer of loss of data when some environmental conditions such as precipitation and snow, cover or make dirty the sensor window. Open-path sensors do not measure directly CO_2 and H_2O mixing ratios but their densities; as atmospheric gas densities could be influenced by fluctuations in pressure, temperature and humidity that generate expansion and contraction of air volume, corrections (*Webb et al.* 1980, WPL) to compensate these effects on measured fluxes are required.

Closed-path analysers can output directly gas mixing ratios, making density corrections (WPL) less important, they don't suffer of data loss due to precipitation and icing but have an high power requirement and are affected by CO_2/H_2O signal tubing attenuation.

2.3 GPP modeling

Photosynthesis can be estimated by different modelling approaches (*Collatz et al.*, 1991; *Cox et al.*, 1998; *Running and Hunt*, 1993; *Veroustraete et al.*, 2002). One of the most widely applied approach for modeling GPP is based on the light use efficiency (LUE) concept, which represents the ratio of carbon biomass production per unit of absorbed light (*Monteith*, 1972; *Horn and Schulz*, 2011). Since some

studies have assessed that light use efficiency is quite stable during a day (*Ruimy et al.*, 1995), it can be used in modelling GPP dynamics at a daily time-step.

This approach stated that GPP is a function of the incident Absorbed Photosynthetically Active Radiation (APAR) and of a light use efficiency (ε) factor (*Monteith*, 1972).

$$GPP = \varepsilon \cdot APAR \tag{2.5}$$

where APAR is the product of the incident photosynthetically active radiation (PAR) and the fraction of photosynthetically active radiation absorbed by vegetation (fAPAR). The magnitude of fAPAR depends on size, density, phenological stage and chemical composition of the canopy. The determination of fAPAR from remote sensing data has matured over a number of years supported by the close relationship between absorbed solar energy and spectral vegetation indices exploiting the visible and near-infrared regions such as the well-known normalized difference vegetation index (NDVI) (*Rouse et al.*, 1974). Since only PAR absorbed by photosynthetic pigments enables photosynthetic processes, whereas the PAR absorbed by photosynthetically inactive elements (e.g., branches, stems and dead leaves) is not used for CO_2 fixation, several recent studies (*Xiao et al.*, 2004; *Zhang et al.*, 2005, 2009) indicate that the use of vegetation indices (e.g. MTCI, *Dash and Curran* 2004) related to canopy chlorophyll content may improve the accuracy of GPP estimation.

Since ε is related to the capacity of a canopy to use light, this parameter is related to the availability of resources for the photosynthetic reactions during the first stage of photosynthesis (see section 2.1.1). ε estimation is one of the most challenging components of the Monteith model; for this reason ε is generally considered as a biome-specific parameter. However, photosynthetic efficiency is known to be also influenced by many factors and thus varies in space and time. Widely used approaches (*Nouvellon et al.*, 2000; *Veroustraete et al.*, 2002; *Heinsch et al.*, 2006) estimate ε as a potential maximum ε, adjusted for unfavourable environmental conditions (e.g. limitations of temperature and humidity).

3 MATERIALS AND METHODS

3.1 Site Description

The study was carried out in a subalpine grassland, in the North-Western Italian Alps, from June 2008 to December 2010. The site is an abandoned pasture located at few kilometres from the village of Torgnon in the Aosta Valley region at an elevation of 2160 m asl (45°50'40" N, 7°34'41" E), (figure 3.1, table 3.1).

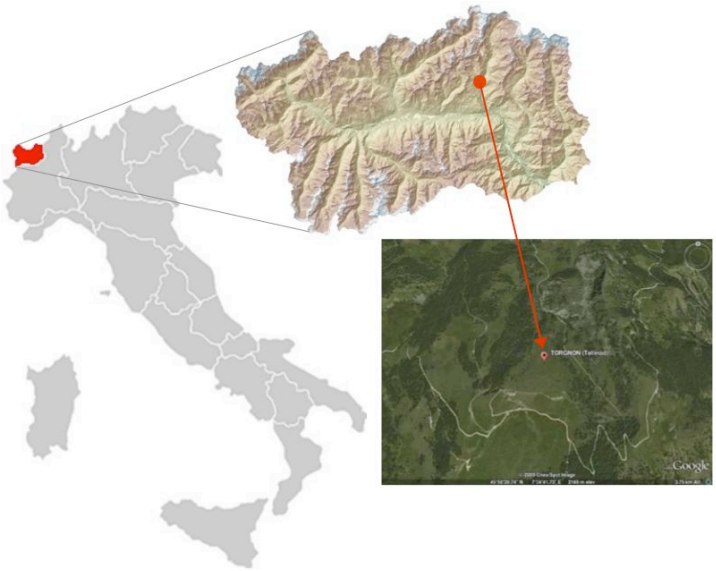

Figure 3.1: *Location of the study site. Red highlighted region is Aosta Valley and red circle on the map indicates the location of the grassland.*

Dominant vegetation of the grassland is composed by *Nardus stricta* L., 35%, *Festuca nigrescens* All. 11%, *Arnica montana* L. 8%, *Carex sempervirens* Vill.

5%, *Geum montanum* L. 5%, *Anthoxanthum alpinum* L.L. 4%, *Potentilla aurea* L. 4%, *Trifolium alpinum* L. 4%. Maximum seasonal Leaf Area Index (LAI) found at the site is near 2.8 (m^2m^{-2}) whereas the soil is classified as Cambisol (WRB classification)

Location	Elevation	Lat./long.	Exposition	Slope	LAI max	Vegetation	Soil	Mean ann. temperature
Torgnon (Italy)	2160 m asl	45°50'40" N, 7°34'41" E	180°	4 °	2.8	*Nardus stricta* 35%	Cambisol	3.1 °C

Table 3.1: *Study site's main characteristics*

The site is characterised as intra-alpine area with semi-continental climate with an annual mean temperature of 3.1°C and mean annual precipitation of about 920 mm (*Mercalli et al.*, 2003). During the study period, the growing season (from June to the end of October) cumulative precipitation varied from a minimum of 172 mm, during 2009 to a maximum of 362 mm during 2010.

Approximately from the end of October or early November to late May the site is snow covered, thus the snow-free period has an average duration of four to five months.

The extent of the homogeneous fetch is approximately 300 m x 300 m around the eddy covariance tower. In a delimited plot of about 15 x 15 m different instruments are installed.

3.2 Data collection

In this section, instruments and their set up are described (Figure 3.2). The instrumental system used during the study was composed by the eddy covariance tower, a weather station that measures additional meteorological variables and a digital camera for monitoring phenology. In the framework of another study, (*Cogliati*, 2011) an automatic hyperspectral system sampling canopy spectral properties was developed and used; here, this system is briefly described, as some of the obtained indices were used in data analysis. Power for the instruments is completely supplied by a set of solar panels. A summary of instruments used is given at the end of this section, in table 3.2.

3.2.1 Eddy Covariance

Eddy covariance method was used to measure the flux of CO_2 and H_2O between the ecosystem and the atmosphere; instrumentation was installed in June 2008 the 20^{th} and measurements continue at present. In this manuscript data from the date of installation to December 2010 are presented.

Instruments were placed at 2.5 m above the ground. The height of the sensors depends on the height of the vegetation, the extent of fetch, the range of wind velocity and the frequency response of the instruments. The higher is the instrument displacement (z_m) of the lower is the sample frequency needed, as eddies dimension gradually increases moving away from the canopy and their frequency decreases; on the other hand the higher is z_m, the bigger is the upwind area influencing the fluxes (*footprint*), a factor that must be accounted for, to not include the fluxes from other ecosystems in the measurements (*Manca*, 2003; *Burba and Anderson*, 2010).

Measurement of wind speed in the three components (*w, u, v*) was performed by a CSAT3 three-dimensional sonic anemometer (Campbell Scientific, Inc., USA), while CO_2 and H_2O vapour air densities were measured by a LI-7500 open-path infra-red gas analyser (LI-COR, Inc., Lincoln, NE, USA). Raw data from both the anemometer and the IRGA were measured at 10 Hz and recorded by a CR3000 datalogger (Campbell Scientific, Inc.). It is recognized that sampling rates between 10 and 20 Hz ensure complete sampling of the high frequency portion of the flux co-spectrum (*Baldocchi et al.*, 2001a).

The choice of an open-path analyser has been lead by some considerations: electric current is not available at the site, precipitations are not abundant, the instrumentation is kept functioning during the winter season.

Calibration of the IRGA was carried out periodically following manual instructions.

3.2.2 Meteorological data

A weather station was installed near the eddy covariance tower to continuously measure meteorological variables useful to compute eddy fluxes and to evaluate the influences of the environmental drivers on the carbon cycle components.

To measure air temperature (Ta) and humidity (RH) we used a HMP45 (Vaisala Inc., Helsinki, Finland), while soil temperature (Ts) was measured with temperature probes type therm107 (Campbell Scientific, Inc.) at four soil depths: 2 cm, 10 cm, 25 cm and 35 cm. Soil water content (SWC) was assessed at two depths, 5 and 30 cm, with soil water reflectometers model CS616 (Campbell Scientific, Inc.), and soil heat flux (G) was measured by HFP01 plates (Hukseflux, Delft, Holland). Net radiation (Rn) was measured with a CNR4 (Kipp and Zonen Corp., Delft, The Netherlands) net radiometer, photosynthetically active radiation (PAR) was assessed by four LI-190 (LI-COR, Inc.) sensors, one above and three below the canopy. Precipitation (PPT) was assessed by an aerodynamic rain gauge ARG100 (Environmental measurements, Ltd, UK), and snow height (HS) was measured with a sonic ranging sensor SR50A (Campbell Scientific, Inc.), finally surface temperature (T_{sur}) was measured with an infra-red temperature sensor SI-111 (Apogee Instruments, Inc.).

All the instruments register data with half-hourly frequency and data were transmitted every day via GPRS modem.

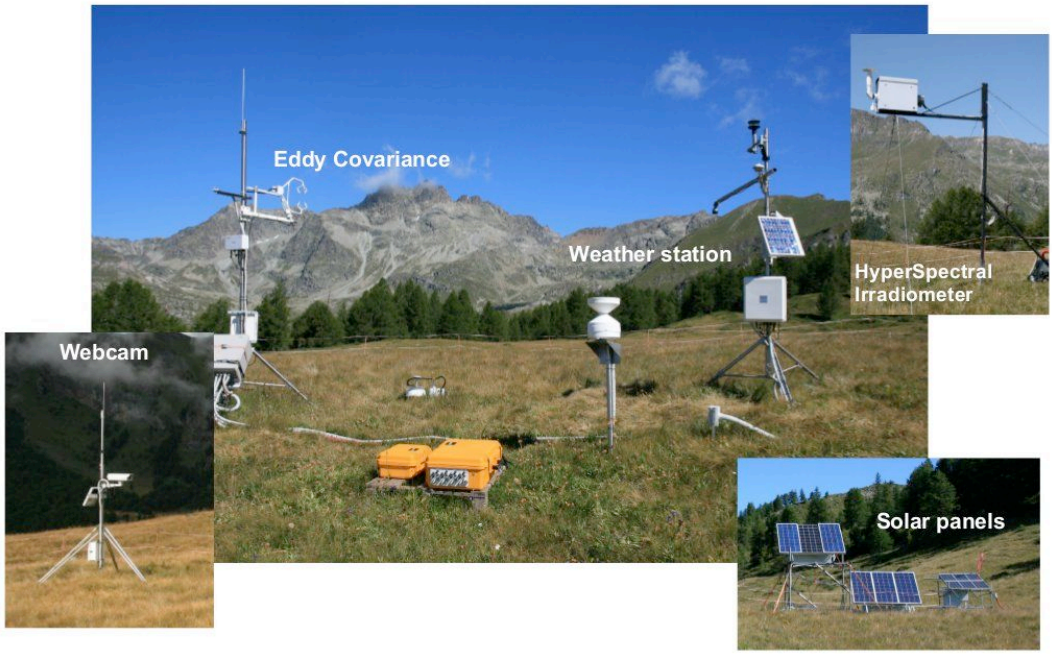

Figure 3.2: *Instrumental system*

3.2.3 Proximal Sensing Measurements

We used a digital camera, model CC640 (Campbell Scientific, Inc.), to remotely track changes in grassland phenology, during the study period starting from May 2009. The digital camera was installed in a weatherproof enclosure at 2.5 m above the ground. The camera was pointed north, and set at an angle of about 20°below horizontal plane following *Richardson et al.* (2007b). Camera focal length was 3.5 mm and the field of view was approximately 79.8 degrees. The scene in the picture takes a great portion (two-thirds) of the vegetation and a little portion (one-thirds) of the background (trees and sky). Desiccant was placed and changed periodically to avoid condensation on box window to form.

The camera was connected to a CR1000 datalogger (Campbell Scientific, Inc.) and provided JPEG images of the same scene (resolution 640 x 480, 0.3 megapixels, with three channels of 8-bit RGB colour information) every hour from 10 am to 4 pm. The camera-JPEG compression mode was set to "None", in order to produce the best quality JPEG files with no artefacts from lossy compression algorithms.

The camera operated with automatic exposure and aperture mode, responding to ambient light levels using the entire image to adjust the exposure settings. Thus, the brightness of any individual pixel was not a direct measure of surface radiance per se. The camera did not record the exposure setting along with the image, thus preventing the conversion of the images into digital numbers (DN) proportional to radiance. An example of digital camera images taken is presented in figure 3.3.

Every day images were transmitted via GPRS modem to ftp. The processing of digital camera images, continuously taken trough the growing seasons, allowed the computation of indices related to the grassland structural seasonal development, as described in the data processing section (3.3.4).

Furthermore in the instrumental plot, an automatic HyperSpectral Irradiometer (HSI) was installed. It is a custom designed instrument (*Meroni et al.*, 2011; *Cogliati*, 2011) developed in collaboration with the Italian National Research Council (IFAC-CNR, Florence). HSI employs a rotating arm to observe alternately the sky and the canopy. A cosine-response optic is used to continuously sample the solar incident irradiance and the irradiance upwelling from the surface. The instrument uses two spectrometers (HR4000, OceanOptics, USA) one operating in the

Figure 3.3: *Examples of JPEG images collected by the CC640 Campbell digital camera during the 2009 growing season.*

visible and near-infrared region of the solar spectrum VNIR (range 400-1000 nm) with a spectral resolution of 1 nm, and the other operating within a narrower spectral interval (700-800 nm) with higher spectral resolution (0.1 nm FWHM, full width at half maximum). Data collected by the first spectrometer allowed the computation of the Vegetation Indices (VIs) as NDVI and MTCI used in the present study, while the second one permit the estimation of Sun-Induced Fluorescence. The HSI was installed in the site from the beginning of June to the end of October in both years.

Variable		Sensor
Eddy covariance		
CO_2 and H_2O		LI-7500 (LI-COR, Inc.)
wind speed/direction		CSAT3 (CampbellScientific, Inc.)
Weather station		
air temperature and humidity	T_a and RH	HMP45 (Vaisala, Inc.)
soil temperature	T_s	therm107 (Campbell Scientific, Inc.)
soil water content	SWC	CS616 (Campbell Scientific, Inc.)
soil heat flux	G	HFP01 plates (Hukseflux)
net ratiation	Rn	CNR4 (Kipp and Zonen)
photosynthetically active radiation	PAR	LI-190 (LI-COR, Inc.)
precipitation	PPT	ARG100 (Environmental measur., Ltd)
snow height	HS	SR50A (Campbell Scientific, Inc.)
surface temperature	T_{sur}	SI-111 (Apogee Instruments, Inc.)
Proximal sensing		
colour index	GI	CC640 (Campbell Scientific, Inc.)
spectral indices	NDVI and MTCI	HSI (*Meroni et al.*, 2011)

Table 3.2: *Instruments summary*

3.2.4 Ancillary data

Various information were available on the structure of the canopy over all the study period.

Vegetative and reproductive phenology of some species (e.g. *Nardus stricta*, *Arnica montana*, *Carex sempervirens*, *Rhododendron ferrugineum*, *Trifolium alpinum*) was observed weekly following an *ad hoc* phenological protocol developed in the framework of the PhenoALP project (http://www.phenoalp.eu/).

Phytomass was collected every two weeks during 2009 and 2010 at 12 plots of 40x40 cm and Leaf Area Index (LAI), and green and total aboveground biomass were determined.

In the same 12 plots, visual observations of canopy percentage of greenness (GVE) and canopy height were collected every week.

Pigment concentrations of the predominant grass (*Nardus stricta*) were determined by extraction in N,N-dimethylformamide (DMF) from plants collected in 4 of the 12 plots, every week during 2010. The absorbance of the extracted material was measured at 663.8, 646.8 and 480 nm by a Cary100 UV-Vis spectrophotometer (Varian, Inc) and chlorophyll a (Chla), b (Chlb) and carotenoid (Car) concentrations were calculated using the extinction coefficients derived by *Porra et al.* (1989).

3.3 Data Processing

3.3.1 Eddy covariance processing

Eddy fluxes were obtained by computing the mean covariance between fluctuations in vertical wind velocity and in CO_2 and H_2O densities, with an half-hour time step. A 30 minutes (or even 60 minutes) averaging period is recognised to be adequate to capture low frequency contributions to flux covariances, but not too long to be affected by diurnal changes in the measured variables. By convention, negative fluxes represent mass and energy movement from the atmosphere to the surface and positive values denote transfer towards the atmosphere and away from the biosphere. Final flux of CO_2 is expressed in $\mu molm^{-2}s^{-1}$ and final flux of H_2O in $mmolm^{-2}s^{-1}$.

Raw 10 Hz data from the eddy covariance system were recorded in a binary data format on a memory card of the CR3000 datalogger. The stored records were processed by using a software (*Manca*, 2003) that calculates half-hour eddy fluxes according to the EUROFLUX methodology (*Aubinet et al.*, 2000).

In particular, some steps are carried out to obtain the final fluxes:

- Linear de-trending: during the averaging period T (30 minutes) a measured variable can show a non-stationary behaviour (i.e., a trend). To eliminate this trend, a linear de-trending is applied based on *Gash and Culf* (1996). This method removes from each *i*-instantaneous record of a measured variable the *i*-value (instantaneous mean) obtained by computing a linear regression trough each half-hour time-series;

- computation of the averages of all measured variables and of the covariance between the turbulent fluctuations of the vertical wind speed and the scalar densities with a half-hour time step;

- three-axis co-ordinate rotation: for each averaging interval of 30 minutes, this algebric operation is computed to align instrumental coordinate system to the mean streamlines of the wind and so that the vertical *w* axis is exactly perpendicular to the mean flow. Moreover a third rotation is computed to eliminate the covariance between *w* and v wind components, if the angle is lower than 10 °(*McMillen*, 1988).

  This operation has the aim to reduce errors due a non-perfect levelled anemometer that can cause a contamination of the vertical component of wind speed by the other two horizontal components (*Kaimal and Finnigan*, 1994; *Manca*, 2003; *Foken*, 2008);

- application of WPL correction: since in this study an open-path gas analyser was used to measure CO_2 and H_2O, this kind of correction is needed (see chapter 2) to correct the fluxes from errors due to temperature and humidity fluctuations. The calculations were made according to *Webb et al.* (1980) and the final CO_2 (Fc), H_2O (E) and sensible and latent heat (H, LE) fluxes were

computed. Additionally the storage term is computed. The storage is important when the thermal stratification of the atmosphere is stable and turbulent mixing is weak, and fluxes from the surface may reach the instrumental system at height z_m slowly, in a time greater than the averaging period T. Under such conditions the storage term becomes non-zero, so it must be added to the eddy covariance measurements. This term considers the time variation of the scalar concentration in the air column under z_m. Nevertheless, generally the storage term is small or even negligible over short crops compared to forests (*Baldocchi et al.*, 2001a).

- calculation of data quality checks: the software calculates quality flags described in the following section.

3.3.2 Data quality and filtering

3.3.2.1 Data quality tests

Quality flags were calculated based on turbulence steady-state criteria and integral turbulence test (*Foken and Wichura*, 1996). In the first case, each calculated 30-min flux is compared to the average of 5 minute flux values of the same half-hour; integral turbulence test characterises whether or not the turbulence is well developed according to Monin-Obukhov' similarity theory (*Aubinet et al.*, 2001), and in practice compares how measured integral turbulence characteristics differ from modelled characteristics. The overall quality level depends on the test that has the worst result: for differences less than 30%, the measurement is flagged as high quality (class 0), if differences are between 30 and 60%, data are considered as good (class 1), whereas more than 60% deviation is flagged as very low quality data (class 2). Furthermore a control is done to exclude data measured with high window dirtiness of the LI-7500 gas analyser (AGC diagnostic >70%).

3.3.2.2 Energy balance closure

The evaluation of the energy balance closure is a good method to assess eddy covariance estimates (*Wilson et al.*, 2002).

This test allows a comparison of turbulent energy fluxes measured with the eddy covariance system (the sensible heat flux, H and the latent heat flux, LE) with energy fluxes obtained by independent methods (net radiation, Rn, ground heat flux, G and energy storage in different ecosystem compartments, S)

In this study the energy balance was firstly assessed by statistical regression of the turbulent fluxes H and LE against the available energy, that can be approximated by the difference between net radiation (Rn) and ground heat flux (G) (*Oke*, 1987), by the following equation:

$$H + LE = Rn - G - S \tag{3.1}$$

where Rn is net radiation measured by the weather station, G is the ground heat flux measured by soil sensors, and H and LE represent sensible and latent heat flux measured by eddy covariance (for all terms units are expressed in Wm^{-2}). The smaller is the difference between the two terms, the higher is the quality of the data used. By passing a linear regression through the data, one can evaluate the percentage of the balance closure by the value of the regression slope. Energy storage (S) values were not considered both in this and the following analysis.

As an alternative method to evaluate the energy balance closure we also applied the energy balance ratio (EBR, (*Wilson et al.*, 2002)) expressed as follow:

$$EBR = \frac{\sum(H + LE)}{\sum(Rn - G - S)} \tag{3.2}$$

Since this method does not compare half-hour data but cumulative energy terms over a large time scale, small scale changes in energy storage tend to become null by summation of any S values over the considered period.

3.3.2.3 Footprint

Footprint analysis allows the definition of the extension of the source area that is actually represented by each flux measurement, i.e."the field of view" of the eddy instruments. In particular the footprint function provides a measure of the fraction of the measured flux that is influenced by a unit point of the upwind surface. Various methods are available to model footprint, in this study the analytical model of

Schuepp et al. (1990) was used. Considering a measurement height z_m, for each horizontal direction (x,y) a footprint function defining the fraction of the measured flux at height z_m generated by the source upwind area at a certain distance (x or y), is computed. The maximum of the footprint function, X_{max}, allows to identify the part of the source area that mainly influences the measured fluxes.

3.3.2.4 Filtering

Beyond the above described data quality checks, spikes or errors due to unfavourable micro-meteorological conditions and to instrument malfunctioning can occur in the half-hour dataset. A filtering procedure was applied to data step by step.

In a first step, data flagged as low quality class (class 2) were excluded from the dataset.

In a second step, an outlier detection technique based on *Papale et al.* (2006) was applied on half-hour flux dataset obtained after a coarse removal of big spikes in the measured variables (i.e. NEE, H, LE or friction velocity) obtained by imposing reliable above and below thresholds. By following *Papale et al.* (2006) the flux dataset was then separated into 13-days blocks and separated for daytime and night-time data. Night-time data were selected as all data below a global radiation threshold of 20 Wm^{-2}. For each block the outlier detection was performed comparing each half-hour value (NEE_i) with the value just before (NEE_{i-1}) and after (NEE_{i+1}). This comparison was based on the median of absolute deviation from the median (MAD).

MAD is defined as

$$MAD = median(|d_i - Md|) \tag{3.3}$$

where d_i is derived from:

$$d_i = (NEE_i - NEE_{i-1}) - (NEE_{i+1} - NEE_i) \tag{3.4}$$

and Md is the median of these differences. A certain value is flagged as spike if

$$d_i < Md - (\frac{z \cdot MAD}{0.6745}) \tag{3.5}$$

or

$$d_i > Md + (\frac{z \cdot MAD}{0.6745}) \tag{3.6}$$

where z is a threshold value, imposed at 4, as in *Papale et al.* (2006).

When a gap is encountered the outlier detection technique can fail identifying a correct value as a spike or not removing an actual spike. In this study the gap treatment was performed as follows:
if NEE in position (*i*) is a non-valid data (NaN), it remains a gap.
if NEE in position (*i-1*) or/and (*i+1*) is a gap, (NEE_i) is compared with the median value of the preceding or subsequent 96 half-hour data.

In the last step, night-time data measured under a certain friction velocity threshold (u_* ms^{-1}) were filtered. This filtering procedure is necessary because during night when photosynthetic uptake of CO_2 is inactive and the net ecosystem exchange represents exclusively respiratory processes, low turbulence condition and limited air mixing can occur. In such condition, the assumptions underlying the eddy covariance theory are not met and the fluxes from the surface may not reach the instruments system (*Goulden et al.*, 1996). As a consequence ecosystem respiration is underestimated and the further cumulative carbon sequestration overestimated.

A current solution to this problem is to filter data using u_*, computed from the eddy measurements, as an indicator of atmospheric turbulence conditions. The filtering technique consists in removing measurements taken under a certain u_* threshold; the generated gaps are replaced with the filling procedure described in the following section. The assumption of this approach is that the night-time flux is ex-

clusively determined by biological activity of the ecosystem and shouldn't depend on turbulence regimes. As it was found that the measured NEE becomes very low as u_* gets close to zero (*Massman and Lee*, 2002), the threshold is identified as that value above which the flux of CO_2 is independent from changes in u_* (3.4).

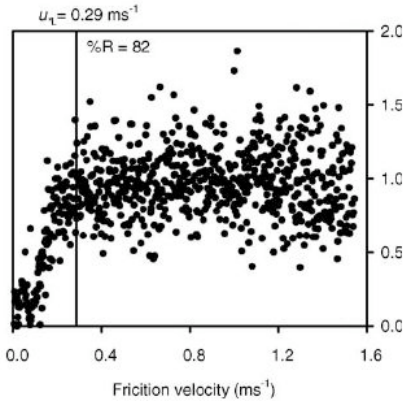

Figure 3.4: *Artificial dataset representing the relationship between night-time NEE versus u_*, from Gu et al. (2005). The vertical line represent the u_* under which data are removed. %R are the percentage of night-time data conserved after filtering*

Literature values of the u_* threshold vary from 0.0 to 0.6 ms^{-1} (*Massman and Lee*, 2002; *Gu et al.*, 2005), and are generally higher for tall vegetation compared to grasslands and croplands (*Papale et al.*, 2006), nevertheless u_* is a site-specific variable and thus threshold should be properly estimated. In this study a u_* procedure is applied based on *Reichstein et al.* (2005) and *Papale et al.* (2006). In summary, the night-time flux dataset is split into six temperature classes of equal sample size (according to quantiles) and for each temperature class, the set is dived into 20 u_* classes. In the original procedure for each temperature class the threshold is identified as the u_*-class where the average night-time flux reaches more than 99% of the average flux at the higher u_*-classes. As an alternative method, in this study we used the Student's t-test to evaluate differences between the average flux of a class and the average fluxes at the higher u_*-classes: the threshold is identified as the first class for which differences from higher u_*-classes are statistically significant (significance level 0.05). Furthermore the threshold is accepted for a particular class if temperature and u_* are not correlated ($|r| < 0.4$). The final threshold is given by the median of the thresholds of the six temperature classes. As u_* distribution

slightly varies as a function of the seasonal period and year considered, the procedure has been tested on different time aggregations, but always considering years separately. The time aggregations tested were: the entire dataset, summer and winter periods separately (i.e. the growing season from June to the end of October, and winter from November to the end of May), periods with similar LAI (e.g. June with September and October and July with August). The average threshold of the different aggregations tested in this study was 0.035 $\pm$ 0.025 ms^{-1}). The u_* filtering was finally performed using the summer (growing season) threshold, that is generally the highest found. A minimum threshold was then imposed to 0.05 ms^{-1}, to be more conservative. The threshold was set to 0.052 ms^{-1} for 2008 and and 0.05 ms^{-1} for 2009 and 2010. These values are similar to those used in another mountain grassland (*Hiller et al.*, 2008).

3.3.3 Gap-filling and partitioning

Together with original gaps in the eddy measurements, artificial gaps due to filtering procedures affect the flux dataset. As a consequence, a gap-filling procedure is necessary to produce daily, seasonal and annual sums of CO_2 exchange. To this aim different methods have been developed. In this study the gap-filling procedure described in (*Reichstein et al.*, 2005) and implemented in the online tool (http://gaia.agraria.unitus.it/database/eddyproc/) was used. We selected this method because it is one of the standardized methods adopted by the Carboeurope-IP project and FluxNet. The gap-filling method is based on both the co-variation of the fluxes with meteorological variables (air temperature, radiation and vapour of pressure deficit, VPD) and the temporal auto-correlation of the fluxes. Therefore, on the basis of the gap type (length, available meteorological variables), missing data were substituted by values obtained on the basis of data measured in similar meteorological conditions (Look Up Tables, LUT) within a time window of $\pm$ 7-14 days, or with values obtained on the basis of data measured in the same time of the day (Mean Diurnal Variation, MDV).

The on-line tool was also used to partition the measured NEE flux into gross primary productivity (GPP) and ecosystem respiration (Reco) by a modelling approach. Flux-partitioning uses only original data (not gap-filled) to derive the con-

stituent flux Reco from the relation between temperature and nocturnal NEE, representative of solely the respiratory process. In this procedure a *Lloyd and Taylor* (1994) regression model is fitted to night-time NEE data (data below the global radiation threshold of 20 Wm^{-2}):

$$Reco(T) = Reco_{,ref} \cdot e^{E_0 \cdot \{\frac{1}{T_{ref}-T_0} - \frac{1}{T-T_0}\}} \tag{3.7}$$

where $Reco_{,ref}$ indicates the respiration at reference temperature, T_{ref}, set to 10°C, E_0 is the activation-energy, T is either air or soil temperature and T_0 is a parameter kept constant to -46.02°C. This function is applied over small window periods of valid data. For each period, the regression parameters and statistics are kept in memory and the best values are used to estimate missing Reco values and day-time Reco. In a next step, half-hour GPP data are derived from the relation

$$GPP = Reco - NEE \tag{3.8}$$

3.3.4 Vegetation Indices

Different vegetation indices derived from the proximal sensing sensors (webcam and HSI) installed at the study site were used in the present study.

3.3.4.1 Digital images VIs

Vegetation indices (VIs) were derived from the processing of 1940 digital images taken from the date of installation in 2009 (DOY 141) to the end of 2010. The images were not selectively edit or artificially enhanced before the analysis; maintaining this level of objectivity could be important because it ensures the repeatability of the methodology at other sites. In order to minimize the angular effect of the canopy hemispherical directional reflectance function (*Chen et al.*, 2000) only the images taken from 11 am to 1 pm were used. A custom R script (*R Development Core Team*, 2011) was used to process and analyse the archived digital image files. Analysis was conducted on one specific "Regions Of Interest" (ROI) of the grassland canopy spanned from the left border of the picture to a reference panel as illustrated in Figure 3.5. The dimension of the ROI was selected to provide a reason-

ably extended spatial sampling of foreground canopy while avoiding the inclusion of the area in the background that might be affected by heterogeneous incident light conditions because of the frequent presence of scattered low clouds and fog in the background.

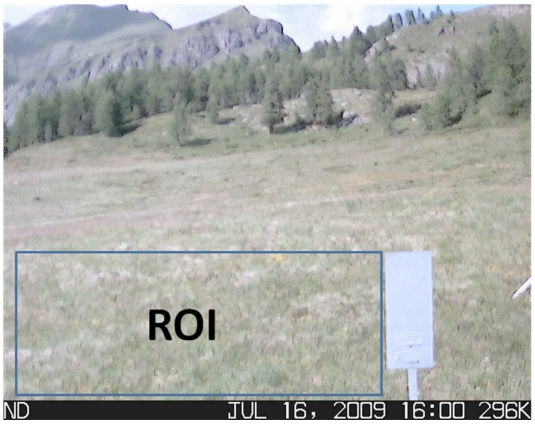

Figure 3.5: *Digital image collected by the CC640 Campbell camera the 16th of July 2009. Blue box denotes the static Region Of Interest (ROI) selected for the study.*

The VIs proposed by *Richardson et al.* (2009a) were computed on each image. In detail, the overall brightness of the ROI (TotalDN) was calculated as:

$$TotalDN = R_{DN} + G_{DN} + B_{DN} \tag{3.9}$$

and was then used to calculate the percent relative brightness of each channel RI (Red), GI (Green) and BI (Blue):

$$RI = \frac{R_{DN}}{TotalDN} \tag{3.10}$$

$$GI = \frac{G_{DN}}{TotalDN} \tag{3.11}$$

$$BI = \frac{B_{DN}}{TotalDN} \tag{3.12}$$

Where R_{DN}, G_{DN}, B_{DN} are the digital number (DN) values of the red, green and blue channel, respectively. The computation of such indices allows to normalize against variations in overall image brightness caused by changes in clouds and solar illumination, as well as image exposure and internal digital camera processing.

Finally, the mean from the three images recorded between 11 am and 1 pm in each day was computed to get a mean daily value of the indices.

Image quality was sometimes adversely affected by rain, snow, low clouds, aerosols, fog, uneven patterns of illumination due to the presence of small clouds (e.g. a part of the image can be overexposed and the target ROI may look darker resulting in a lower value of VI, or vice versa). The result is that smooth trajectories of the digital camera VIs related to canopy greenness were sometimes interrupted by a sharp increase or decrease of the VI values, lasting for one or few days. Therefore, the time series were filtered to suppress unusual high or low values with a recursive outlier removal filtering. In a first step outliers were removed on the basis of MAD (eq. from 3.3 to 3.6); in a second step a cubic smoothing spline was fitted to data and the residuals between the value of each daily VI and the corresponding value of the smoothing spline were calculated (*Bradley et al.*, 2007). A particular day i was considered as "good", and then retained for further analysis, if

$$|residual(VI_i - spline_i)| < \mu + 3\sigma \tag{3.13}$$

where μ is the mean of the residuals and σ is their standard deviation. The algorithm described above was recursively applied at the digital camera VIs time series until no outliers were detected (with a maximum of 10 loops).

3.3.4.2 HyperSpectral Irradiometer VIs

The vegetation indices computed from HSI reflectances and used in this study are the Normalised Difference Vegetation Index (NDVI) (*Rouse et al.*, 1974), that gives a measure of the greenness of the vegetation and the Meris Terrestrial Chlorophyll vegetation Index (MTCI), (*Dash and Curran*, 2004) that is related to the canopy chlorophyll content. NDVI is calculated as

$$NDVI = \frac{r_{800} - r_{680}}{r_{800} + r_{680}} \tag{3.14}$$

where r_{800} and r_{680} are the reflectance values at the specified wavelength (nm), and MTCI is calculated as:

$$MTCI = \frac{r_{753.75} - r_{708.75}}{r_{708.75} + r_{681.25}} \tag{3.15}$$

where $r_{753.75}$, $r_{708.75}$ and $r_{681.25}$ are the reflectance values at the specified wavelength (nm).

3.4 Data Analysis

3.4.1 Extraction of phenophases from ecosystem processes and canopy greenness

Information on grassland phenology were extracted with different methods starting from the seasonal time-series of both the flux components NEE and GPP, representing phenology of ecosystem processes, and the digital camera GI, representing phenology of the canopy greenness.

The extraction of the phenophases from the NEE time-series was based on the carbon uptake period (CUP). This approach defines the beginning (BGS) and the end of the growing season (EGS) as the date when the ecosystem switched from a source to a sink and the reverse. Different literature methods were used to identify these dates: in the first approach we identify BGS and EGS as the zero-crossing dates after which NEE turns definitively from daily negative values to positive ones in spring and from negative to positive values in autumn (*Piao et al.*, 2008); in the second approach zero-crossing dates are defined as above but using a moving average with a 5-day window (*Richardson et al.*, 2009b); in the last approach a regression line is passed between NEE and DOYs using a subset of spring and autumn data (15 days for each period). The BGS or EGS date is identified by the DOY for which the predicted NEE has value 0 (*Baldocchi et al.*, 2005).

For GPP, BGS and EGS dates were defined as the DOY at which the GPP time series reaches the 10% of the spring development and the 90% of the autumn decrease; the curve was previously smoothed with a cubic spline.

This last method was also applied to the seasonal time-series of GI, to extract BGS and EGS of the structural development.

In summary while NEE thresholds are physiologically defined, GPP and GI phenological dates represent development stages of the considered variables and are thus comparable.

3.4.2 Light-response curves

Because photosynthesis is driven by light, but the way NEE responds to changes in photosynthetic photon flux density (PPFD) could changes within vegetation types and seasons, the light-response curve was analysed to describe the relation between NEE and PPFD at Torgnon grassland in different periods of the growing season. Various functions describing this relation exist; in this study we used a rectangular hyperbolic light-response function (on the basis of Michaelis-Menten equation, *Falge et al.*, 2001):

$$NEE = \frac{F_{MAX}\ \alpha\ PPFD}{\alpha\ PPFD + F_{MAX}} + Reco \tag{3.16}$$

where F_{MAX} ($\mu molCO_2$ $m^{-2}s^{-1}$) is the maximum CO_2 flux at infinite light (also referred as maximum assimilation, A_{MAX}), PPFD ($\mu molm^{-2}s^{-1}$) is photosynthetic photon flux density, α the apparent quantum yield and Reco the ecosystem respiration.

As PPFD increases, photosynthetic CO_2 assimilation increases: NEE values change from positive values of night respiration towards negative ones, passing through a point where CO_2 uptake exactly balances CO_2 release. This value is called the light compensation point. Above the light compensation point photosynthetic assimilation increases linearly with PPFD and the velocity of this rise (i.e. the slope of the linear relation between NEE and PPFD) is the maximum quantum yield of photosynthesis. Quantum yields vary from 0, where no PPFD is used, to 1, where all the absorbed light is used for photosynthesis. In the intact leaf, measured quantum yields for CO_2 fixation vary around 0.04 and 0.06 (*Taiz and Zeiger*, 2010). At higher PPFD, the photosynthetic response to light reaches a saturation, and CO_2 assimilation assumes its maximum value, F_{MAX}. Further increases in incident light don't affect the photosynthetic rate (see *Taiz and Zeiger* 2010).

Light-response curves were calculated by fitting day-time (data above a global

radiation threshold of 20 Wm^{-2}), half-hour NEE data, measured during the growing season from June to October, to the equation 3.16; Model parameters were estimated using the simulated annealing algorithm implemented by the function `optim()` (Stats package) of the statistics software R (*R Development Core Team*, 2011). Because the structure and function of the vegetation vary over the season, the fitting was performed dividing the dataset in five time periods for each year, characterized by different LAI values. According to *Ruimy et al.* (1995) the flux of CO_2 at a PAR value of 2000 $\mu molm^{-2}s^{-1}$ was assumed as a proxy of F_{MAX}.

3.4.3 Multi-scale analysis of environmental controls over carbon exchange

In the analysis of the relations between environmental drivers and CO_2 fluxes, the spectral approach of wavelet coherence analysis was applied. This method is widely employed in climatology (*Torrence and Compo*, 1998), but poorly represented in carbon fluxes studies (*Vargas et al.*, 2010). As ecosystem processes are influenced by weather and climatic fluctuations at multiple temporal scales, linear relationships between meteorological variables and flux components are often weakly able to reveal the underlying controls. The analysis in the time-frequency domain has been demonstrated useful for the evaluation of the correlation between the periodicities of time-series of environmental factors and those of carbon cycle processes (*Vargas et al.*, 2011).

In the context of spectral analysis, the advantage of wavelets, compared to Fourier transform method, is the ability to capture the frequency content of a time series as a function of time and to discern discontinuous non-stationary events present in the signal, such as rain pulses or heat waves. By using wavelets the spectral properties of the time-series of interest are analysed as divided into several parts trough a fully scalable modulated window that is shifted along the signal, and for every position the spectrum is calculated. This process is over-repeated with windows of different sizes: the final result is a collection of time-frequency representations of the signal, with different time resolutions.

The method described is the continuous wavelet transform (cwt), that is expressed

by:

$$W_n(s) = \left(\frac{\delta t}{s}\right) \sum_{n^i=0}^{N-1} x_n \psi_0^* \left(\frac{n-n^i}{s/\delta t}\right) \tag{3.17}$$

where x_n is a discrete signal of length N, sampled at δt interval, ψ_0^* is the complex conjugate of the scaled and translated mother wavelet (or basic wavelet), and s is the scale at which the transform is applied. The mother wavelet is the base function from which transformations are computed. Different type of mother wavelet exist, one of the most used is the Morlet wavelet (*Grinsted et al.*, 2004).

Based on the continuous wavelet transform, the wavelet coherence analysis (wco) allows to identify regions of local correlations between two time-series as a function of frequency.

In this study wavelet coherence analysis was applied to investigate coherencies between the periodicities of eddy CO_2 fluxes with air temperature, soil temperature, SWC, and PAR, the key environmental variables of the ecosystem studied, at the hourly, daily, weekly, monthly and seasonal time scales. The half-hour time series of carbon flux and environmental drivers measured from June 2008 to December 2010 were used.

The wavelet coherence analysis was computed using the function `wco()` of the R package Sowas (SOftware for Wavelet analysis and Synthesis, http://tocsy.agnld.uni-potsdam.de/wavelets/). This function uses time-series data as input to estimate the wavelet coherence of two variables, based on the Morlet mother wavelet. This application evaluates correlations between the two processes with respect to time and scale. Correlations varied between 0 (absence on coherence) and one (full coherence).

3.4.4 GPP modelling

A LUE modelling approach (*Monteith and Unsworth*, 2008) was used to simulate GPP at site level.

LUE models assume that carbon fixation is a linear function of the incident photosynthetically active radiation absorbed by a canopy (APAR) and the Light Use

Efficiency (LUE), which represents the conversion efficiency of absorbed energy to fixed carbon, following the relation firstly proposed by *Monteith* (1972):

$$GPP = \varepsilon \cdot APAR \tag{3.18}$$

This approach requires an estimate of APAR that can be derived from the relation:

$$APAR = fAPAR \cdot PAR \tag{3.19}$$

where fAPAR is the fraction of absorbed photosynthetically active radiation used by the vegetation for photosynthesis.

In this study, the widely known LUE model MOD17 (*Heinsch et al.*, 2006), which is the algorithm of the MODIS daily photosynthesis product (MOD17), was used:

$$APAR = fAPAR \cdot PAR \cdot f(meteo) \tag{3.20}$$

To estimate fAPAR, GI derived from digital images was tested, while PAR was derived from measurements at the meteorological station. In particular fAPAR was estimated as a linear function of GI:

$$fAPAR = a_0 + a_1 \cdot GI \tag{3.21}$$

As in MOD17, ε term was estimated as ε_{max}, the maximum conversion efficiency for the ecosystem, adjusted for weather conditions which are expressed by linear ramp functions of limiting factors: minimum air temperature Ta_{Min} and VPD. These functions vary linearly (*Jolly et al.*, 2005) between 0, (when daily variable value is lower than a minimum threshold under which photosynthesis is assumed as fully constrained), and to 1 (when daily variable value is above an upper threshold indicating that photosynthesis is completely unconstrained) as a consequence of suboptimal temperatures and water availability for photosynthesis.

As an example, the function used to describe the influence of Ta_{Min} is expressed as (figure 3.6):

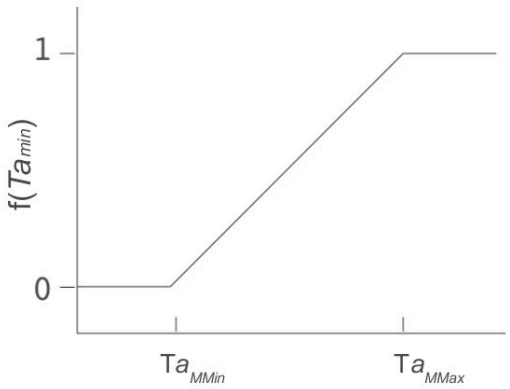

Figure 3.6: *Example of the function used to describe the influence of minimum air temperature, f(Ta_{Min}) on photosynthesis. Ta_{MMin} and Ta_{MMax} indicate thresholds between which the constrain is assumed to vary linearly from 0 (total constrain) to 1 (no constrain).*

$$f(Ta_{Min}) = \begin{cases} 0, & \text{if } Ta_{Min} \leq Ta_{MMin} \\ \frac{Ta_{Min}-Ta_{MMin}}{Ta_{MMax}-Ta_{MMin}}, & \text{if } Ta_{MMax} > Ta_{Min} > Ta_{MMin} \\ 1, & \text{if } Ta_{Min} \geq Ta_{MMax} \end{cases} \tag{3.22}$$

where f(Ta_{Min}) is the daily indicator for minimum temperature, bounded between 0 and 1, Ta_{Min} is the observed daily minimum temperature, Ta_{MMin} and Ta_{MMax} indicate thresholds between which the constrain varies linearly.

For VPD, the daily indicator function f(VPD) assumes the value of 1 when the daily VPD is lower than the minimum threshold (VPD_{Min}), and assumes the value of 0 when daily VPD is greater than the maximum threshold (VPD_{Max}) over which VPD forces stomatal closure.

In this study, different model formulations were tested to investigate the importance of other environmental controls, i.e. snow, Ts_{Min} and SWC in limiting photosynthesis in this ecosystem. In particular, in separated steps, we tested: the application of a snow presence/absence threshold,

$$GPP = \varepsilon_{max} \cdot f(Ta_{Min}) \cdot f(VPD) \cdot (a_0 + a_1 \cdot GI) \cdot PAR \cdot snow(1,0) \tag{3.23}$$

and the use of $f(Ts_{Min})$ in place of $f(Ta_{Min})$ and $f(SWC)$ in place of $f(VPD)$. For each model formulation, model parameters were estimated against the daily GPP derived from eddy covariance measurements during the 2009 growing seasons and the best-fit model parameters were then used in the simulation of 2010 GPP to evaluate the applicability of the method. In table 3.3 estimated parameters for different model formulations are summarized.

formulation	$MOD17_{original}$	$MOD17_{snow}$	$MOD17_{Ts}$	$MOD17_{SWC}$	$MOD17_{Ts,SWC}$
parameter set					
ε_{max}	■	■	■	■	■
Ta_{MMin}	■	■		■	
Ta_{MMax}	■	■		■	
VPD_{Min}	■	■	■		
VPD_{Max}	■	■	■		
Ts_{MMin}			■		■
Ts_{MMax}			■		■
SWC_{Min}				■	■
SWC_{Max}				■	■
a_0	■	■	■	■	■
a_1	■	■	■	■	■

Table 3.3: *Parameter sets for different model formulations*

Model parameters were estimated using simulated annealing algorithm, implemented with the R function `optim()`. First guess parameters for the optimization on 2009 dataset were derived from MOD17 biome-specific values for grassland (*Heinsch et al.*, 2003). Root mean square error (RMSE) between observed and modelled data was used as cost function. 300 loops (over 20000 simulating annealing iterations) for each model formulation were performed and the main fitting statistics (r^2, RMSE, and the modelling efficiency, EF) were computed to extract the best parameter set for 2010 simulation. The same statistics were then used to evaluate the overall accuracy of different models formulation (Janssen and Heuberger, 1995).

To evaluate the parameter uncertainty of MOD17 driven by GI, a chi-square (χ^2) test was performed comparing the sum of squared error (SSE) of the best-fit parameter set with SSEs of each 300 parameter set (deriving from the 300 loops). The test excludes the parameter sets significantly different from the best-fit one. The effect of parameter uncertainty on modelled GPP was evaluated comparing GPP

estimates obtained with all parameter sets not excluded by the χ^2-test (*Richardson et al.*, 2010).

Finally, to evaluate the use of GI as a proxy of fAPAR in GPP modelling at ecosystem level, we compared MOD17*original* driven by GI with the same formulation of the model driven by traditional radiometric VIs computed from HSI data, NDVI and MTCI, as substitute of GI.

4 RESULTS

4.1 Eddy covariance data

4.1.1 Data coverage

Eddy covariance system provided continuous measurements of CO_2 Net Ecosystem Exchange (NEE) starting from 2008 June the 20*th* to the end of 2010. Together with gaps, caused by instrumental failure occurred during the study period, the exclusion of low quality data and the filtering procedure, described in section 3.3.2, also introduced gaps in the flux dataset.

Data coverage during the three growing seasons was always in the range reported by other studies in similar ecosystem (*Wohlfahrt et al.*, 2008b; *Zeeman et al.*, 2010): 61% in 2008, 51% in 2009 and 58% in 2010. During 2009 data coverage was slightly lower because of a gap of several days occurred in June, caused by a breakdown. In table 4.1 data coverage for the whole year, and the winter and growing season periods are reported. As expected, data coverage during winter was inferior compared to summer because of more frequent instrument malfunctions (e.g snow cumulated on LI-7500 window) and because of the higher occurrence of low quality data on the basis of turbulence steady-state criteria and integral turbulence test (see chapter 2). The filtering techniques described in section 3.3.2.4 excluded data flagged as low quality (class Qc 2), spikes detected on the basis of MAD and night-time data below a given u_* threshold (0.052 ms^{-1} in 2008 and 0.05 ms^{-1}in 2009 and 2010); the relative contribution of each of the above mentioned steps on the total amount of gaps is showed in figure 4.1.

During the growing season, on average, original gaps were lower than 15% (ex-

	Year (data %)	Growing Season (data %)	Winter (data %)
2008		61	
2009	46	51	43
2010	45	58	35

Table 4.1: *Data coverage (% of valid data) for different periods. In 2008 the system was installed on June the 20*th *so data coverage referred to the whole year and winter period is not reported*

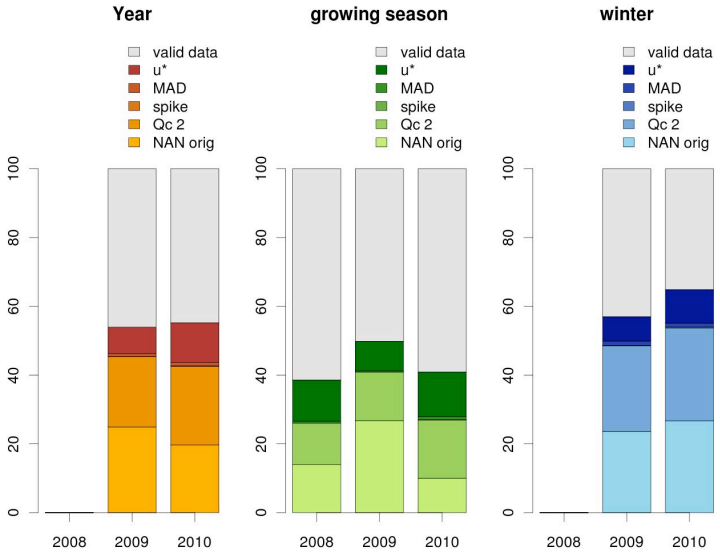

Figure 4.1: *Data coverage for different periods: from left to right, the complete dataset (Year), the growing season period and the winter period. Original gaps and those generated by the different filtering procedures are outlined by the colour palette. Grey area indicates the percentage of valid data.*

cept for 2009), quality test rejected nearly 10.6% of the data and 11.3% was excluded by the u_* threshold, while the outliers represented a low portion of rejected data (<1%).

4.1.2 Energy balance closure

The energy balance closure is an indicator of the quality of eddy covariance data. Figure 4.2 shows the scatter plot between the available energy (Rn-G) against the turbulent energy fluxes (H + LE) for the entire study period, from June 2008 to

December 2010. The coefficient of determination (r^2) and the slope of the regression line were considered separately for the growing season and the snow-covered period.

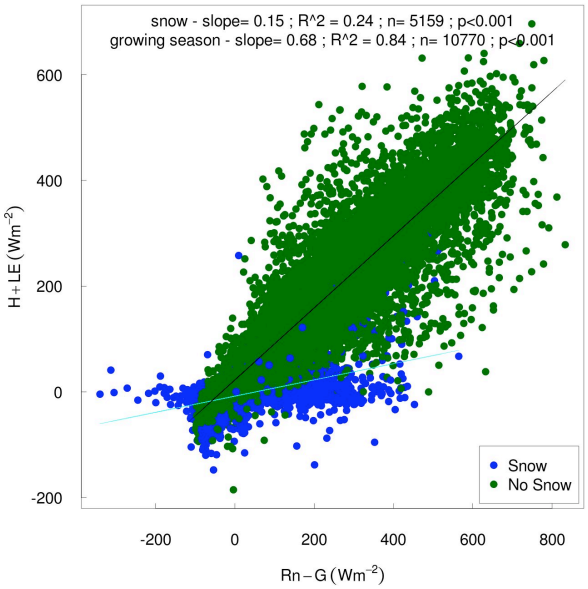

Figure 4.2: *Energy balance closure in the observation period (2008-2010). Green points represent the growing season measurements, points in blue indicate measurements during the snow covered period; The r^2 and slope (closure) of the regression lines are also reported.*

Green points represent snow-free period measurements and showed an r^2 of 0.84 with an overall balance closure of 68%. Points in blue belong to the snow covered period, for which the regression line has an r^2 of 0.24 and a slope of 0.15. Energy balance closure during the growing season was good and fell within values found in other grasslands (*Hiller et al.*, 2008) and was similar to that reported for 22 FLUXNET sites (*Wilson et al.*, 2002) on an annual basis. On the contrary energy balance closure during winter was poor, since the energy balance concept is hardly applicable to a snow covered surface (*Armstrong and Brun*, 2008).

Results from EBR (equation 3.2) computed on growing season data showed an overall closure of 0.80. This results further outlined a good accuracy of the measured turbulent fluxes.

4.1.3 Flux footprint

In figure 4.3 the footprint calculated considering all data belonging to the quality class 0 and 1 and above the critical u_* threshold is presented. In the polar plot the the distribution of the peak flux footprint X_{max} was computed by 11.25°sectors for the growing seasons 2009 and 2010, and divided into percentiles for each particular sector.

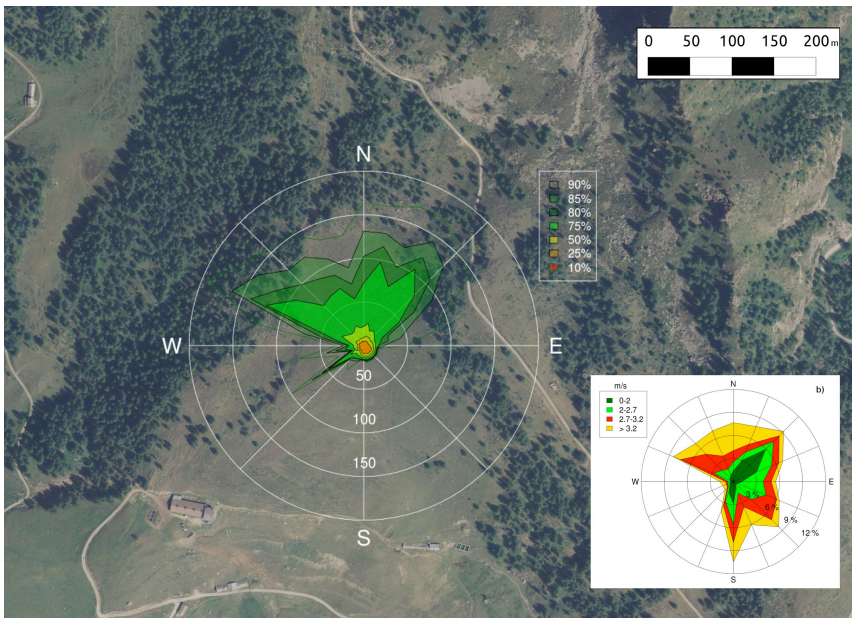

Figure 4.3: *a) Airborne image of the site with the polar plot of the distribution of the peak flux footprint (X_{max}) computed by 11.25°sectors for the growing seasons 2009 and 2010. The isolines and different colours represent the percentiles of the distribution of X_{max} in a particular sector. (b) Wind rose: wind frequencies are expressed in percentages and computed by 11.5°wind sectors for the growing seasons 2009 and 2010. The colours in each sector indicate the wind speed class.*

The overall median of X_{max} was 17.8 m. During daytime the median X_{max} was lower (14.23 m). These values are in agreement with other analysis conducted with a similar experimental set-up over alpine grasslands (*Marcolla and Cescatti*, 2005). Considering daytime fluxes, about 90% of the fluxes was emitted by an area within 40 m around the eddy covariance system.

Since wind direction, its daily cycle and velocity influence the flux footprint (*Hiller*, 2007), the mean diurnal variation of wind field and X_{max} was analysed

and showed in figure 4.4.

During day-time hours, the wind blew up-valley from south-east sector and X_{max} represented a small source area. During night-time, wind direction changed in some cases to down-valley from north-northwest sector and source area was wider. Overall, during the growing season winds mainly came from the south-eastern quadrants, while in winter,the north-northwest directions occurred most frequently. In all the study period during the transition from day-time to night-time (and vice-versa) wind speed (figure 4.4 c) was slower compared to that of central hours of the day. Generally higher velocities were found during the growing season compared to winter period.

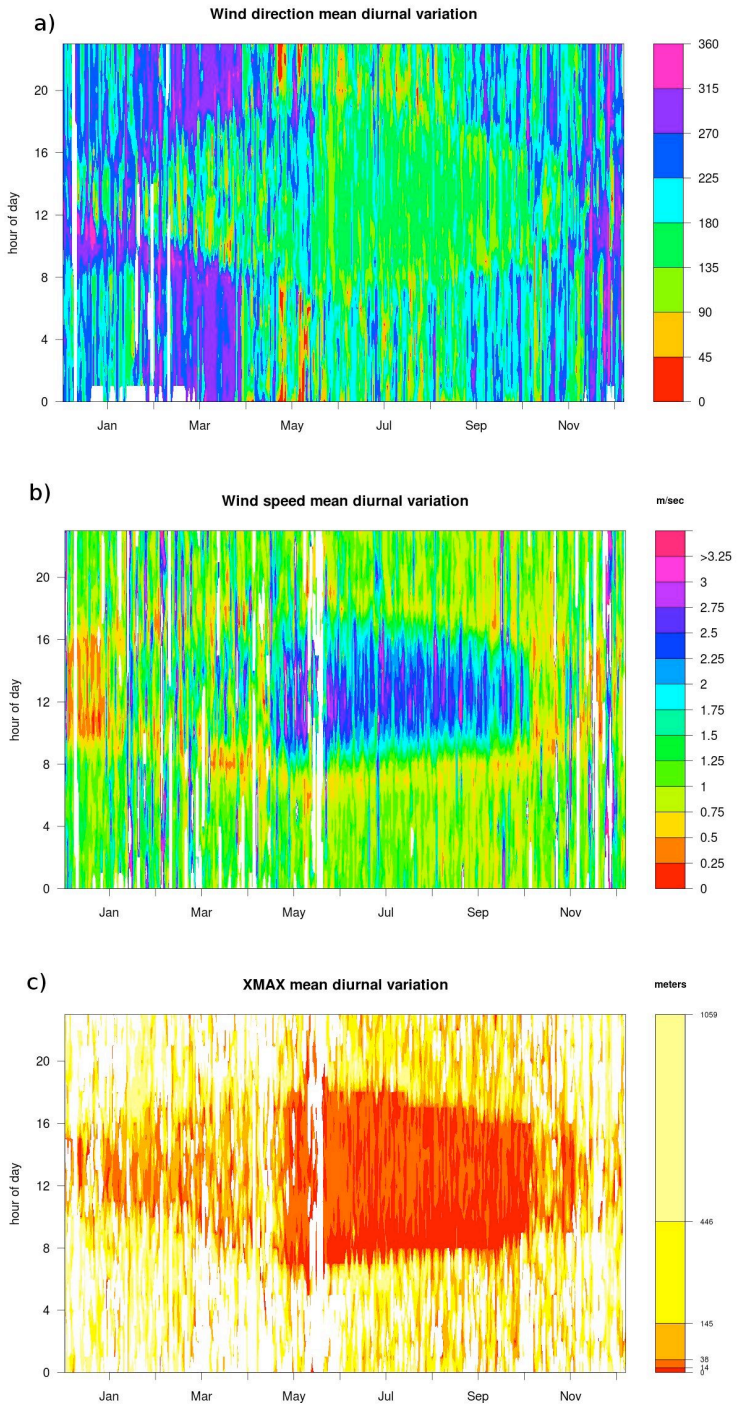

Figure 4.4: *Mean diurnal variation of wind direction, wind speed and X_{max} during the study period. a) Colours indicate 45° sectors of wind directions; b) Colours indicate wind speeds c) Colours indicate distances of the peak flux footprint from the eddy covariance system. White areas are generated from gaps in the dataset.*

4.2 Seasonal and interannual variability in weather, carbon fluxes and vegetation indices

4.2.1 Meteorological variables time-courses

Figure 4.5 shows the time course of the majors meteorological variables during the study period. As measures started June 20*th* in 2008, analysis and comparisons involving the winter period do not include 2008 data.

Snow covered the grassland for approximately seven months each year (figure 4.5 a); considering hydrological years, snow covered period lasted 210 days (from 28 October 2008 to 26 May 2009), in winter 2008-2009 and 202 days (from 02 November 2009 to 23 May 2010) in winter 2009-2010. Snow height differed markedly between the two hydrological years: maximum height measured in 2008-2009 was 1.74 m, while was 0.95 m in 2009-2010. The first year was particularly snowy compared to the average (1.10 m) of the period 1927-2005 in the same area (*Mercalli et al.*, 2003). Moreover maximum Snow Water Equivalent (i.e. the amount of water contained within the snowpack computed multiplying snow density [Kg/m^3] and snow depth [m]), was 708 we (water equivalent, mm) in 2008-2009 and 378 we (mm) in 2009-2010.

The seasonal pattern of mean diurnal values of incident PAR (figure 4.5 b) was similar between the different years.

As expected for an alpine environment, air temperature (figure 4.5 c) showed wide fluctuations from winter to summer and varied from a minimum of -16.8 $\pm$ 0.65°C (two years averages) in December to a maximum of 20.8 $\pm$ 0.37 (three years averages) in August.

Soil temperature (figure 4.5 d) varied from a minimum of to 0.5 $\pm$ 0.9°C reached in January to 16.5 $\pm$ 2.0°C, in August. During winter under the snow cover T*s* had more mild and stable values and remained constantly decoupled from air temperature. Just after the snow melt soil temperature exhibited a strong rise from mean values of nearly 1.4 $\pm$ 1.1 °C (three days before snow-melt average) to 6.4 $\pm$ 0.7 °C, (three days after snow-melt average), reaching in few days values similar to those of air temperature. Considering both air or soil temperature, no remarkable

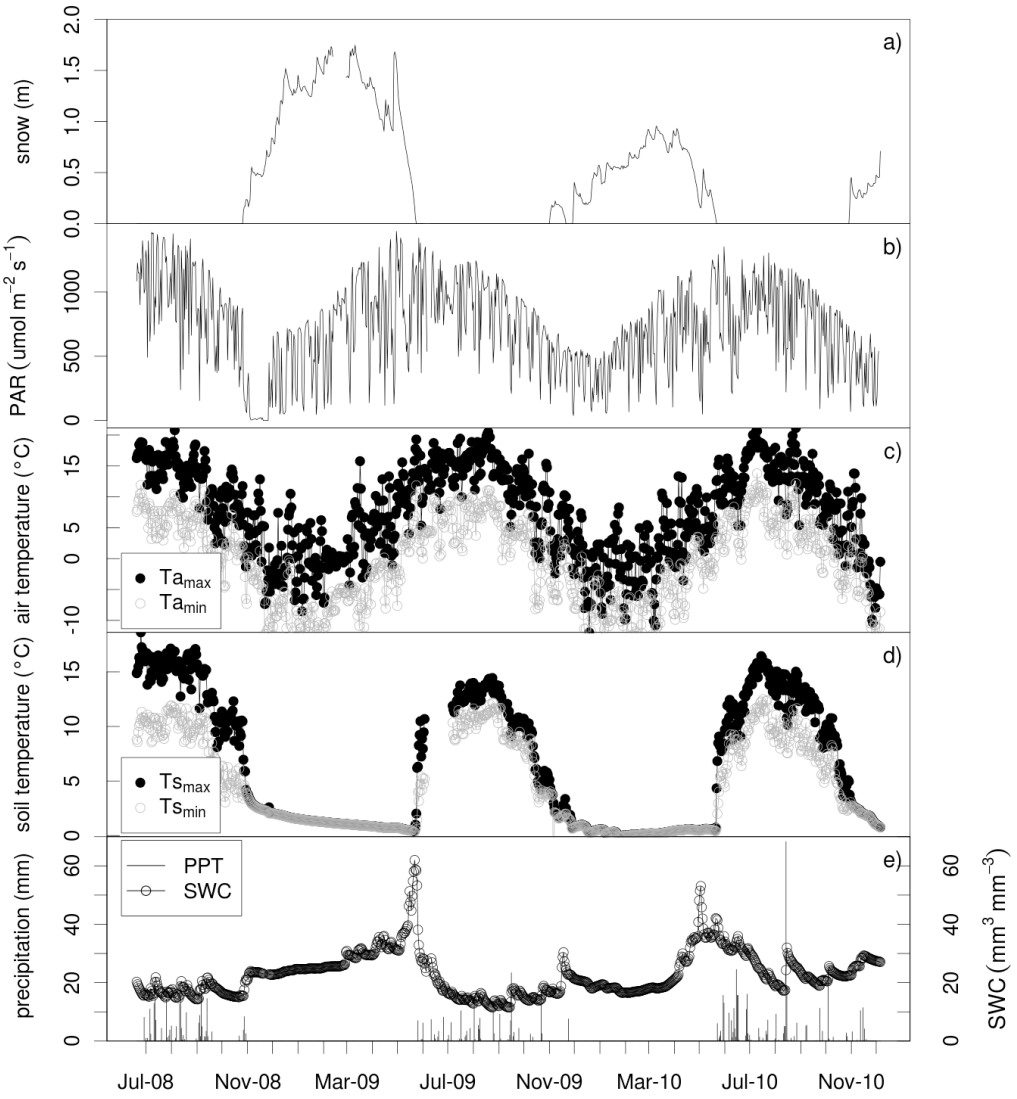

Figure 4.5: *Meteorological variables time-courses in three years of measurements, from June 2008 to the end of 2010. a) snow height (m); b) PAR ($\mu molm^{-2}s^{-1}$); c) air temperature (°C); d) soil temperature (°C); e) SWC (mm^3mm^{-3}) and precipitation (mm).*

differences were found among years.

With snow, precipitation (figure 4.5 e) during the snow-free period, was the meteorological factor that markedly differed among the three years in terms of total amount; in 2008 (from June 20*th*) growing season total precipitation amounted to 229 mm, in 2009 to 172 mm, while 2010 was the year with highest total precipita-

tion, that amounted to 362 mm. 2010 precipitation regime was the most similar to long term average (400 mm, 1927-2001) in the same area (*Mercalli et al.*, 2003), while 2009 was particularly below average. Overall, the seasonal pattern of PPT distribution was quite similar among years.

SWC varied with precipitation inputs during the growing season and had constant values under snowpack in winter (figure 4.5 e). Seasonal SWC was generally higher in 2010, the year with more precipitation, with a mean value of 24.6 mm^3mm^{-3}, compared to a mean of 16.0 mm^3mm^{-3} and 15.0 mm^3mm^{-3} in 2008 and 2009, respectively. SWC exhibited a typical peak around the day of snow melt when it reached the highest value (59.4 mm^3mm^{-3}) in 2009, the year with the highest snow height and SWE. In summary, considering the whole growing season, SWC was higher in 2010, while 2009 was the year with the greatest input of water, coming from snow melt, at the beginning of the growing season.

4.2.2 Temporal dynamics of carbon fluxes

In figure 4.6, time-courses of daily gap-filled NEE and the derived flux components Reco and GPP are presented.

The three growing seasons were clearly characterised by the net uptake of CO_2 (negative NEE values) and by high values of GPP. Winter periods were characterised by low and constant respiratory fluxes.

The ecosystem started to be a net sink on average on DOY 153-154 (June 2*nd*-3*rd*) and turned to a source meanly on DOY 285-290 (October 12*th*-17*th*). An accurate description of the dates representative of different phases in the carbon flux courses, are given in section 4.3.

The three growing seasons showed quite similar peak values of daily GPP, NEE and Reco (8.2 $\pm$ 0.3 $gCm^{-2}d^{-1}$, -4.7 $\pm$ 0.3 $gCm^{-2}d^{-1}$, 4.43 $\pm$ 0.2 $gCm^{-2}d^{-1}$ for GPP, NEE and Reco respectively).

The seasonal variations of fluxes were also similar within years. NEE and GPP showed fast increases in spring, just after snow-melt (May 26*th* and 23*th* in 2009 and 2010 respectively, figure 4.5), rapidly reaching the peak in early July (13*th*-14*th*) and thus indicating an intense carbon uptake at the beginning of the season. On the contrary during the second part of the season (i.e. from the middle of July) the

decreasing rate of both GPP and NEE was clearly slower compared to the increasing one. Reco had a more gradual course, similar in both the beginning and the end of the growing season and reached peak value meanly in the middle of July.

Little differences in this general course occurred in the three years. In 2009, during the second part of the season, GPP showed some episodes of flattening of the decreasing trend and recovery (around DOY 270, September 27*th*). Moreover at the end of the growing season higher amount of positive pulses of NEE (also verified through independent measurements of ecosystem respiration with chamber method, data not shown) appeared in 2008 and 2010 compared to 2009.

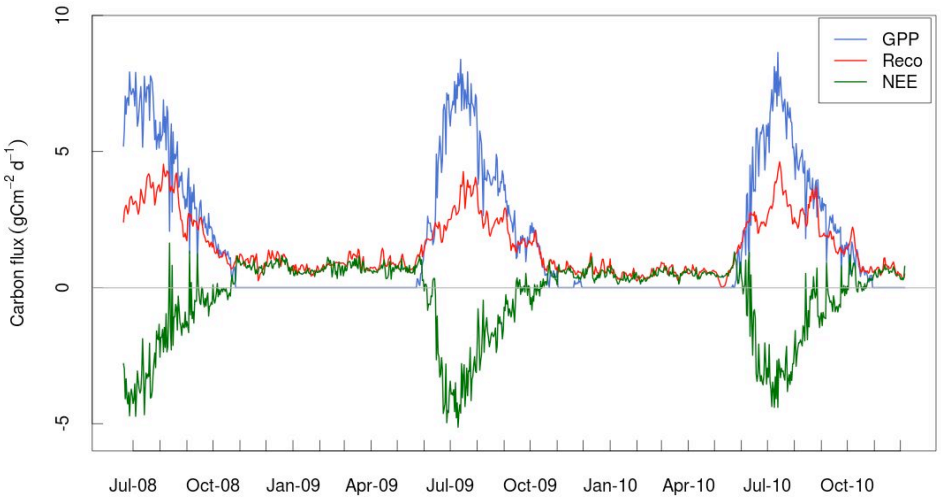

Figure 4.6: *Carbon flux components time-course from June 2008 to December 2010. The green line represents daily Net Ecosystem Exchange (NEE), while red and blue line represent, ecosystem respiration (Reco) and Gross Primary Production (GPP), respectively. Values are expressed as daily sums($gCm^{-2}d^{-1}$).*

This differences can be more easily detected in the seasonal cumulative values of GPP, NEE and Reco and resulted in a higher carbon sequestration during growing season 2009, compared to other years.

Cumulative values computed on a monthly aggregation, from June to October, are presented in figure 4.7. As mentioned above, 2009 growing season had generally higher measured NEE, higher GPP and lower Reco, a difference that appeared almost for each considered month (not in September). Seasonal integrated values

(snow-free period) of NEE, Reco and GPP were respectively: -195.6, 343.8 and 539.5 gCm^{-2} in 2008, -221.78, 343.8, 565.6 gCm^{-2} in 2009 and -182.14, 355.3, 537.4 gCm^{-2} in 2010.

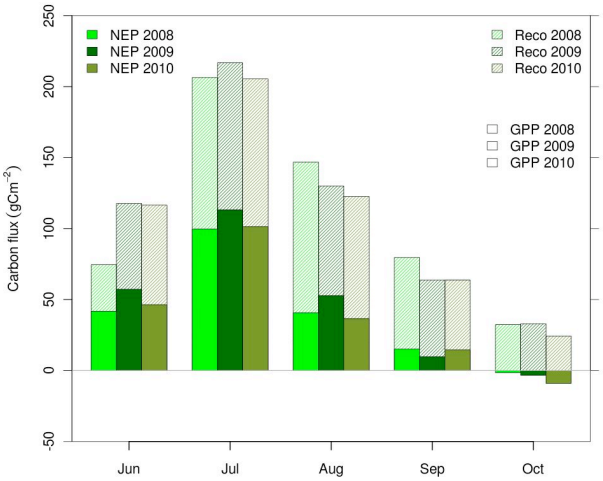

Figure 4.7: *Monthly Carbon flux components; The total height of the bar represents the monthly GPP, the dashed portion the monthly Reco, and the colour filled portion is the net difference of the two, i.e. NEP (Net Ecosystem Production). The term NEP is here the opposite of NEE and is introduced to facilitate graphical reading.*

Annual cumulative NEE, GPP, and Reco for the years 2009 and 2010 are presented in figure 4.8. As previously described, GPP and NEE increasing rates were high at the beginning of the growing season just after snow-melt (SM dates are indicated as vertical lines in figure and 4.8 and 4.9), and became slower after the middle of July. Considering inter-annual variability, despite differences in final cumulative values, the rate of CO_2 sequestration and release in the first part of the growing season is fairly constant within years. In figure 4.9, which focuses only on NEE, 2008 data are added to outline the similar shape of cumulative curves in the three years.

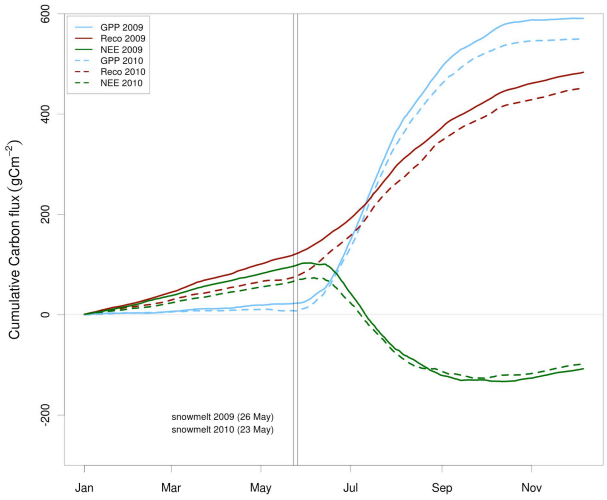

Figure 4.8: *Annual cumulative NEE, Reco, and GPP (in green, red and blue respectively), from January to December. Vertical lines indicate the dates of snow-melt: May 26*th *and 23*th *in 2009 and 2010 respectively.*

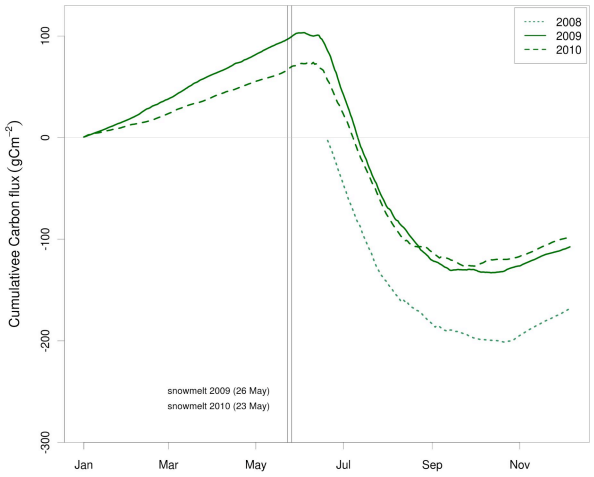

Figure 4.9: *Annual cumulative NEE in three measurements years from January (June in the case of 2008) to December. Vertical lines indicate date of snow-melt: May 26*th *and 23*th *in 2009 and 2010 respectively. The shift towards lower values for 2008 data is caused by the absence of measures in the period form January to June that results in a lack of positive cumulative values (i.e. cumulative winter respiration)*

From the comparison between meteorological and flux data (figure 4.5 and 4.6) it is clear that the snow cover duration was a constraint for the period available for photosynthesis; nevertheless, while in spring photosynthetic activity is physically limited by the snowpack, in autumn GPP and NEE reached minimum values before the first snow fall. Furthermore, from this comparison emerged that the year 2009, with lower precipitation and SWC during the growing season but higher snow height in the preceding winter and thus an higher water input in the beginning of the growing season, had higher GPP, NEE, and lower Reco, compared to 2010, the year with more precipitation and SWC.

Moreover the recover of carbon sequestration observed during late summer-autumn 2009, was associated with favourable values of some meteorological factors (rain pulses after a dry period and warmer temperature); in the other years, during the same period, weather conditions (PPT, temperature, PAR) were generally more limiting.

A more exhaustive analysis of the environmental controls over carbon exchange is given in section 4.4.

4.2.2.1 Light-response curves

Light-response curves analysed by means of the rectangular hyperbolic light-response function (see section 3.4.2) allowed the characterisation of seasonal changes of NEE in the response to PPFD (Photosynthetic Photon Flux Density). Figure 4.10 presents light-response curves calculated for the three growing seasons and divided for different months, characterised by different LAI values (1.3 in June, 2.5 in July, 2.1 in August, 1.2 in September, no LAI data for October). The light-response curve for June 2009 was not reported as for this month the available data were not sufficient to obtain a good fit (see section 4.1).

The response of measured NEE to PPFD, has a clear course from June to October which remains constant within years. During the early part of the growing season, F_{MAX} (considered at 2000 μmolm^{-2}s^{-1}, $F_{MAX2000}$) reached its maximum value in July (-12.45, -12.2 and -11.45 μmolm^{-2}s^{-1}, in 2008, 2009 and 2010 respectively) and decreased gradually from August to October (minimum values -2.45, -1.13, -1.49 μmolm^{-2}s^{-1} for 2008, 2009 and 2010 respectively). During the senescence

period (September-October) light saturation was reached at very low PPFD values (below 200 μmolm^{-2}s^{-1}).

The quantum yield, α (molmol^{-1}), found in July, the month with the highest F_{MAX}, was 0.03, 0.076, 0.078 in 2008, 2009 and 2010 respectively. The values found for both F_{MAX} and α were similar to those reported in other studies in C3 grasslands and in particular in mountain grasslands (*Flanagan et al.*, 2002; *Wohlfahrt et al.*, 2008a)

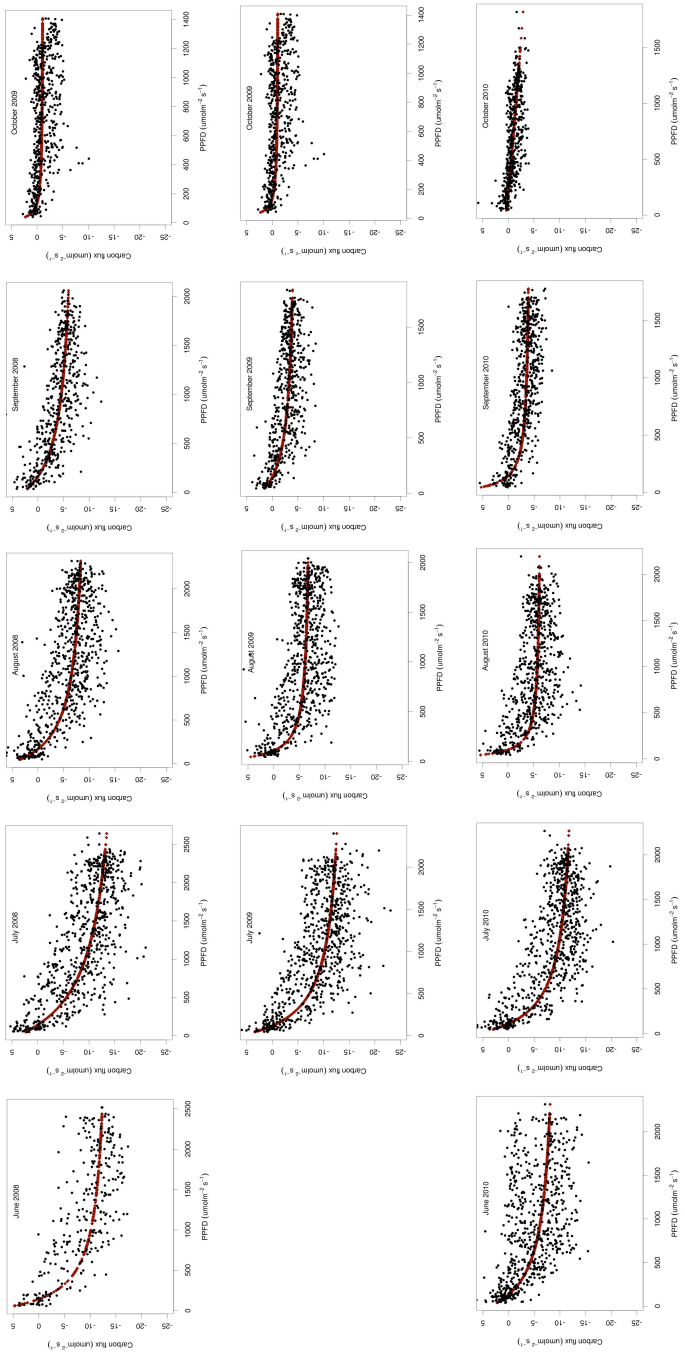

Figure 4.10: *Examples of light-response curves of NEE plotted for different months from 2008 to 2010. Fitted curves represent the rectangular hyperbolic light-response function as described in section 3.16.*

4.2.3 Colour and spectral Vegetation Indices time-courses

Time-series of midday GI derived from the analysis of digital camera images (section 3.3.4), computed for the growing season 2009-2010, are reported in figure 4.11, while NDVI and MTCI obtained from HSI data are showed in figure 4.12. GI began rising slowly immediately after the snow-melt and at faster rate after DOY 165-170 (June the 14-19*th*), reaching its maximum in July (around DOY 200, July the 15-19*th*) in both years. Over the subsequent weeks, GI showed a steady decline due to late summer and autumn yellowing. In 2009, from DOY 270 (September the 27*th*) a pronounced localised increases in GI was observed. Spectral VIs (i.e. NDVI,

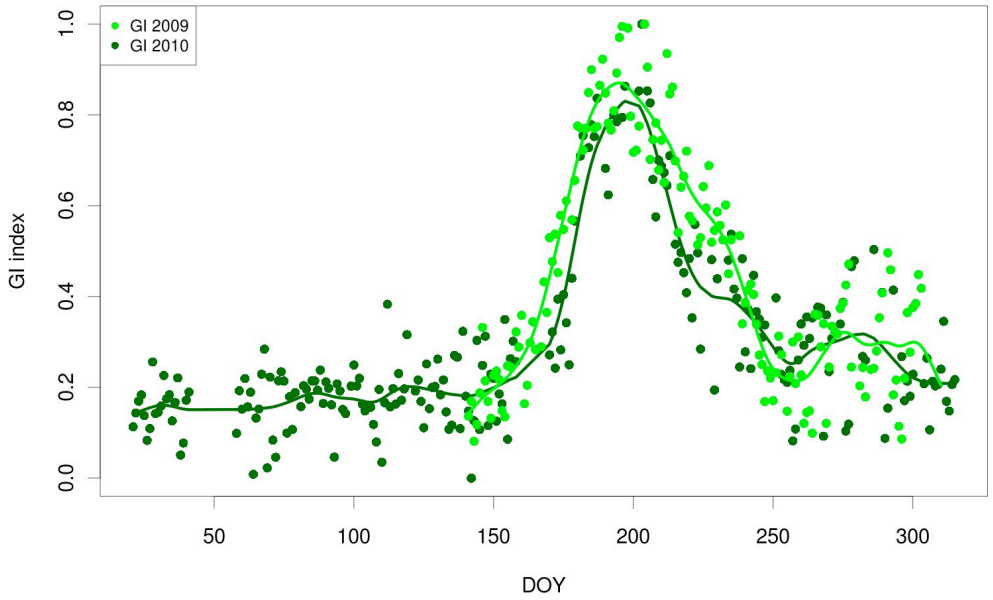

Figure 4.11: *Daily time-course of the Greenness Index (GI) computed from continuous digital camera imagery. 2009 (May-Dec) and 2010 (Jan-Dec) data are plotted in light-green and dark-green respectively. Lines are cubic smoothing splines fitted to data.*

MTCI) and GI were in accordance during spring rise and early summer (DOY 150 to 200); in late summer and autumn 2009 and 2010 (from DOY 200), MTCI and GI showed similar patterns, while NDVI decreased more slowly than both MTCI and GI.

In both years, springtime increases in GI were quite synchronous with GPP, but

afterwards, GPP tended to anticipate changes in canopy greenness (see section 4.3).

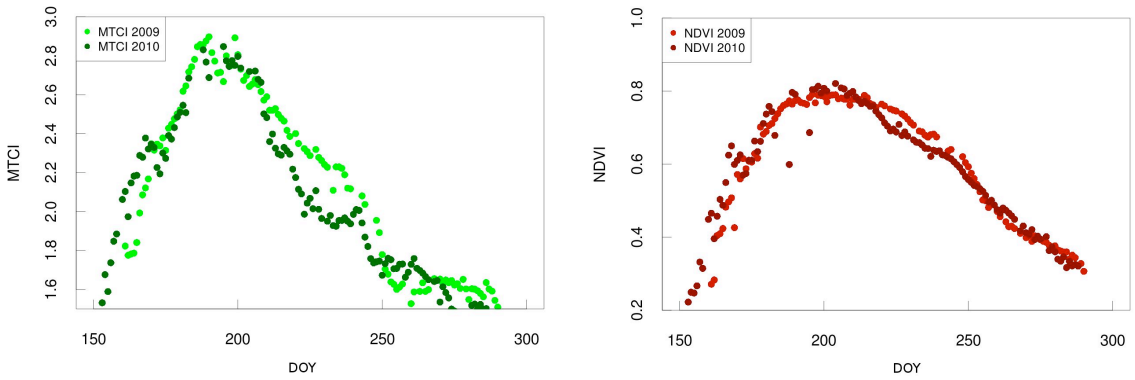

Figure 4.12: *Summer (Jun-Oct) daily time-course of MTCI and NDVI, derived from continuous HyperSpectral Irradiometer (HSI) measurements. (left) MTCI: 2009 and 2010 data are plotted in light-green and dark-green respectively; (right) NDVI: 2009 and 2010 data are plotted in light-red and dark-red respectively.*

The increase in GI occurred in autumn 2009 reflected the weaker but detectable increase in GPP that occured in correspondence to rain pulses (around DOY 270) with a subsequent increase in SWC and warm of soil temperature. This autumnal recovery was detected also by MTCI but not by NDVI.

In order to evaluate the strength of the relations between Vegetation Indexes, ancillary measurements and GPP, correlation matrix are reported in table 4.2 and 4.3.

	Total Biomass	Green Biomass	LAI	GVE
GI	n.s	0.68	0.77	0.72

Table 4.2: *Pearson correlation coefficient between GI derived from digital camera imagery, and ancillary data (Total Biomass, Green Biomass, LAI and GVE (i.e. Greenness Visual Estimation)); n.s. represents non significant correlation.*

	GI	GPP	MTCI	NDVI
GI	1	0.79	0.82	0.69
GPP		1	0.95	0.83
MTCI			1	0.87
NDVI				1

Table 4.3: *Correlation matrix between GI derived from digital camera imagery, GPP and VIs computed from spectral signatures collected with the HSI (MTCI, NDVI).*

4.3 Phenology of ecosystem processes and canopy greenness

The methods applied to derive phenological metrics from canopy function and greenness development, allowed to obtain begin of season (BGS) and end of season (EGS) dates for each variable and year considered, and consequently gave the possibility to derive the length of the growing season (GSL) from a functional and structural point of view. In table 4.4 phenological dates extracted from NEE, GPP and GI and the date of snow-melt (SM) and snow-in (SI) are presented. The snow free period lasted approximately 160 days in each season. This number can slightly change ($\pm$ 2 days) deriving snow-melt and snow-in events on the basis of the snow depth sensor measurements (target area with a radus of approximately 50 cm) or looking at digital camera images (representative of a wider area). The ecosystem turned to a sink approximately 6 and 11 days after snow-melt in 2009 and 2010 respectively, and the CUP lasted 132 days in 2009 and 137 days in 2010. Regarding GPP, in 2009 10% of the spring development was reached 3 days after snow-melt and 4 days in 2010. As previously described, GI dynamic was in agreement with

GPP, but the increase in GI was slight slower in early spring with a 10% of maximum canopy greenness reached 5 and 7 days (2009 and 2010 respectively) after 10% of GPP; while in autumn canopy greenness reached 90% of decrease 13 and 9 days after GPP.

	Method	CUP 1	CUP 2	CUP 3	GPP 10%	GI 10%	Snow		
BGS	2009	152	152	153.5	149	154	SM	2009	146
	2010	154	154	156.9	147	154		2010	143
EGS	2009	284	284	285.4	290	303	SI	2009	306
	2010	295	291	292.3	295	304		2010	303
GSL (days)	2009	132	132	131.9	141	149	snow-free (days)	2009	160
	2010	141	137	135.9	148	150		2010	160

Table 4.4: *Phenological dates extracted from carbon components (NEE and GPP) and canopy greening (GI) dynamics. BGS is the beginning, EGS the end and GSL the length of the growing season. Methods used are described in section 3.4.1; CUP refers to Carbon Uptake Period methods used to derive dates when NEE turns from positive to negative (BGS) values and the reverse (EGS). For both GPP and GI, 10% of the spring development and the 90% of the autumn decrease were considered as BGS and EGS. In Snow columns, dates of snow-melt (SM), snow-in (SI) and days of snow-free period are reported. GSL and snow free period duration are computed as differences between BGS and EGS and between SM and SI, respectively.*

4.4 Multi-scale analysis of environmental controls over carbon exchange

Results of the wavelet coherence analysis allowed to identify correlations between environmental variables and photosynthesis at multiple time scales, along the time domain (i.e.days of the year) during three years of measurements (from June 2008, to December 2010). Input data were the half-hourly values and the time-scales considered varied from daily (1 day) to nearly annual (256 days). Figures from 4.13 to 4.16 showed the results of wavelet coherence analysis between GPP and air temperature, soil temperature, SWC and PAR. Only GPP was analysed, rather than NEE, because the latter is governed by factors that control both assimilation and respiration components.

In plots (from 4.13 to 4.16), Y-axis represents the time scales in days, expressed

with an exponential annotation; the coloured areas represent regions of similar periodicities of two time-series power spectrum, from values of high coherence in red, to values of low coherence in blue. The black line on the margins of the plots, delimits the cone of influence (i.e. the region not influenced by edge effects), outside which the results are unreliable and have to be interpreted carefully (*Vargas et al.*, 2010).

The big blue areas in the plots represent the winter periods, during which GPP was null. For each plot different coherences at different temporal scales along the time domain can be identified.

Regarding air temperature (figure 4.13) the highest coherence with GPP was at the daily scale during the growing season, indicative of a common diel cycle between temperature and photosynthesis during the period of plant activity. Some localised coherences at larger scales (16-32 days) can be identified during senescence period, representing similar decreasing patterns of late summer/autumnal temperature and GPP. Nevertheless no clear seasonal control of air temperature on photosynthesis appears from this analysis.

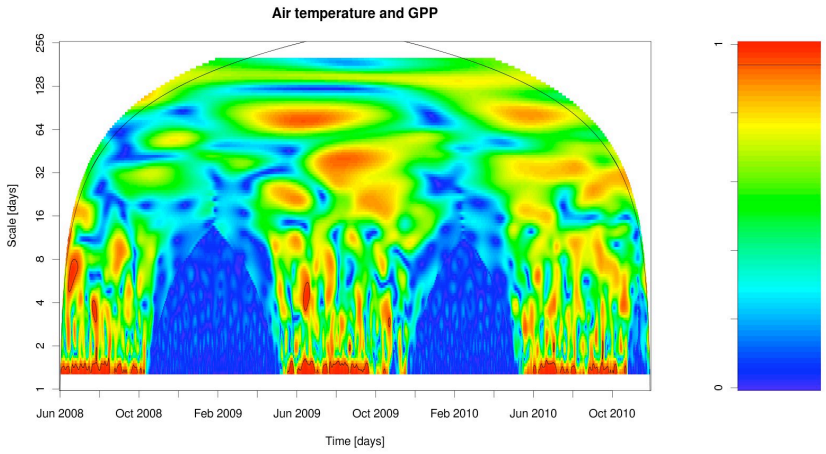

Figure 4.13: *Wavelet coherence analysis between GPP and air temperature from June 2008 to December 2010. On the Y-axis the time-scale is reported. Low to high coherence values are represented in the color palette from blue to red.*

Like air temperature, soil temperature (figure 4.14), within the growing season exhibited a daily cycle coherence with photosynthesis. Moreover the seasonal and

inter-seasonal coherences are generally higher compared to air temperature ones, underlying that soil temperature and GPP time-courses were strictly coupled by the presence of snow on ground; since snow covered the ground for approximately seven months during winter (see section 4.2.1), under the snow pack photosynthesis was inhibited and soil remained isolated from air maintaining mild, constant values (figure 4.5 d). Just after the snow-melt soil temperature exhibited a fast rise, that probably positively influenced carbon uptake processes. The coherence related to snow-melt rise is evident in figure 4.14, in both 2009 and 2010 (while in 2008 measurements started after the snow-melt): a wide (4-32 days) red area was evident just after the end of the winter period (early June). At the end of the 2009 growing season a 16-32 days coherence can be identified: this correlation could be explained by the synchronous recovery of GPP and soil temperature flattening during the decreasing trend occurred in late summer/autumn 2009.

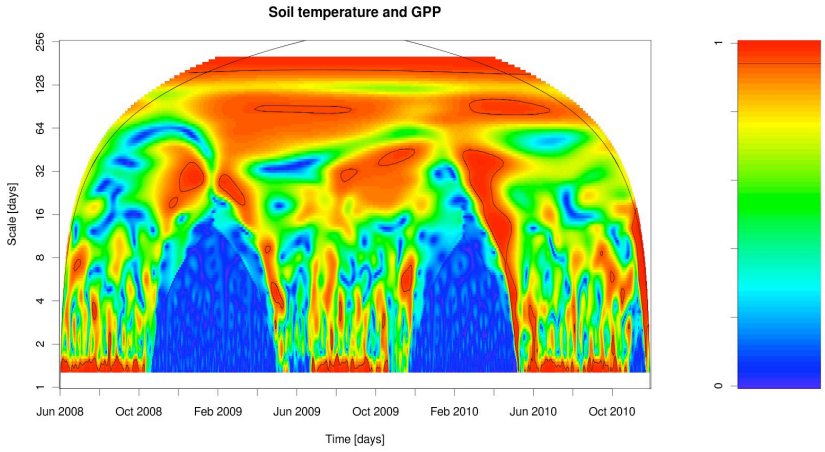

Figure 4.14: *Wavelet coherence analysis between GPP and soil temperature from June 2008 to December 2010. On the Y-axis the time-scale is reported. Low to high coherence values are represented in the color palette from blue to red.*

Wavelet coherence analysis between SWC and GPP (figure 4.15) showed principally two kind of relationships: on the seasonal scale and on the weekly (from 2 to >8 days) scale, while no daily cycle was detected. Seasonal coherence reflected that also SWC and GPP had similar time-course regulated by the snow period just like soil temperature. The weekly coherence showed that during the growing season,

relationships between soil moisture and GPP were evident in specific periods, associated with rainfall inputs producing effects on GPP lasting some days. Moreover a 16-32 days weak coherence appeared in spring 2009, the year with the higher input of water in soil during the snow-melt (see section 4.2.1), but it is not present in the following year, that had lower water input at the early beginning of the season.

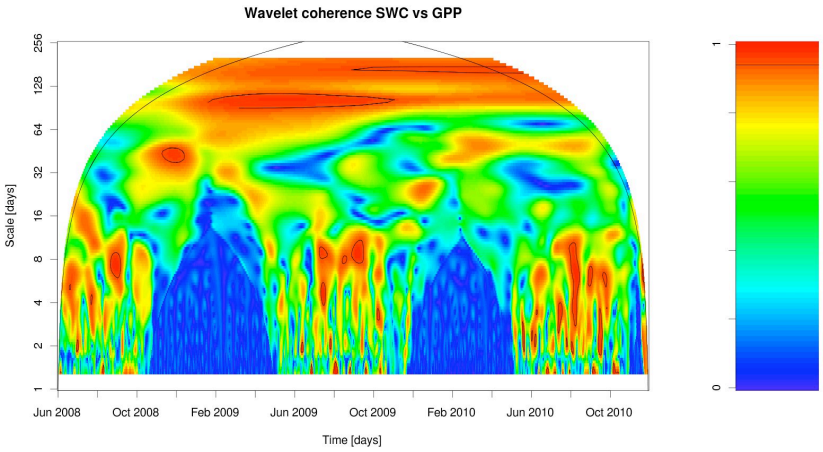

Figure 4.15: *Wavelet coherence analysis between GPP and Soil Water Content (SWC) from June 2008 to December 2010. On the Y-axis the time-scale is reported. Low to high coherence values are represented in the color palette from blue to red.*

Finally wavelet coherence between GPP and PAR is showed in figure 4.16. As expected PAR had a great influence on the daily cycle of photosynthesis, within the growing season. Nevertheless on the inter-seasonal time scale, the coherence between GPP and PAR is again limited by the snow presence on ground. Indeed, PAR started to rise early (around February) while vegetation remained decoupled from ambient light conditions until the snow-melt in late May: thus when GPP began to rise PAR had already reached its maximum value. A localised coherence was found at the end of the 2010 growing season, that was likely due to the simultaneous decrease of GPP and PAR (i.e cloudy conditions) in that period (e.g. 91 μmolm^{-2}s^{-1} around DOY 267).

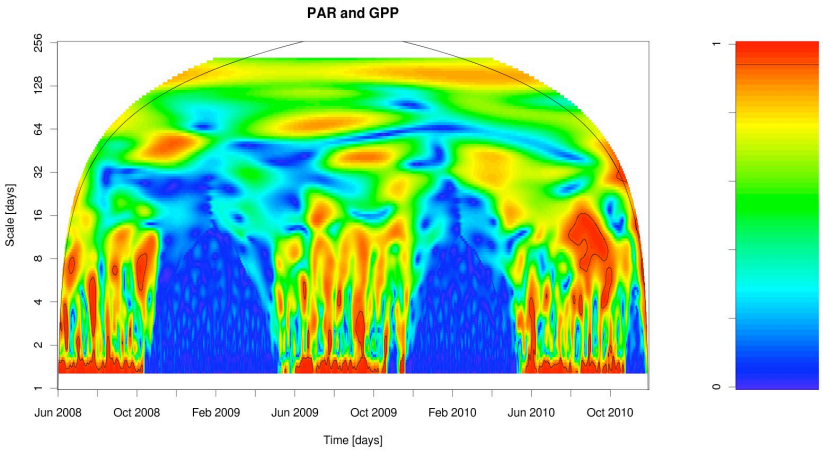

Figure 4.16: *Wavelet coherence analysis between GPP and Photosynthetically Active Radiation (PAR) from June 2008 to December 2010. On the Y-axis the time-scale is reported. Low to high coherence values are represented in the color palette from blue to red.*

4.5 GPP modelling

The statistics of all model formulations tested in this study are presented in table 4.5 and 4.6.

Results showed that colour indices (i.e. GI), when combined with meteorology can be successfully used for the description of the dynamics of daily GPP. In figure from 4.17 to 4.24 the results of 2009 and 2010 simulations are presented, compared to daily GPP observed data, for different model formulations. As previously described, the digital camera was installed in May 2009, and thus model optimisation was performed starting from this date, while in 2010 GPP was simulated starting from January.

Good results were obtained in 2009 optimisation (RMSE= 0.981 $gCm^{-2}d^{-1}$, EF=0.828, r^2=0.829) using the $MOD17_{original}$ formulation 3.4.4 and temporal variability of daily GPP is quite well represented (figure 4.17 (left)); nevertheless when applying the optimised parameters to simulate 2010 GPP (figure 4.17 (right)), a systematic overestimation was observed at the beginning of the season: with this formulation, the optimised parameters lead to an estimation of the beginning of photosynthetic activity highly in advance, compared to measured data. Air temperature and PAR used in $MOD17_{original}$ started to increase, when vegetation was still

covered by snow: the decoupling of vegetation processes from the meteorological factors considered in this MOD17 formulation, caused the divergence in estimated and measured early season data. Considering cumulative GPP while in 2009 observed and modeled data were quite in agreement (observed GPP=565.0 gCm^{-2}, modeled GPP=553 gCm^{-2}) in 2010 the model overestimated GPP by more than 100 gCm^{-2} (observed GPP=537.4 gCm^{-2}, modeled GPP = 646.4 gCm^{-2}).

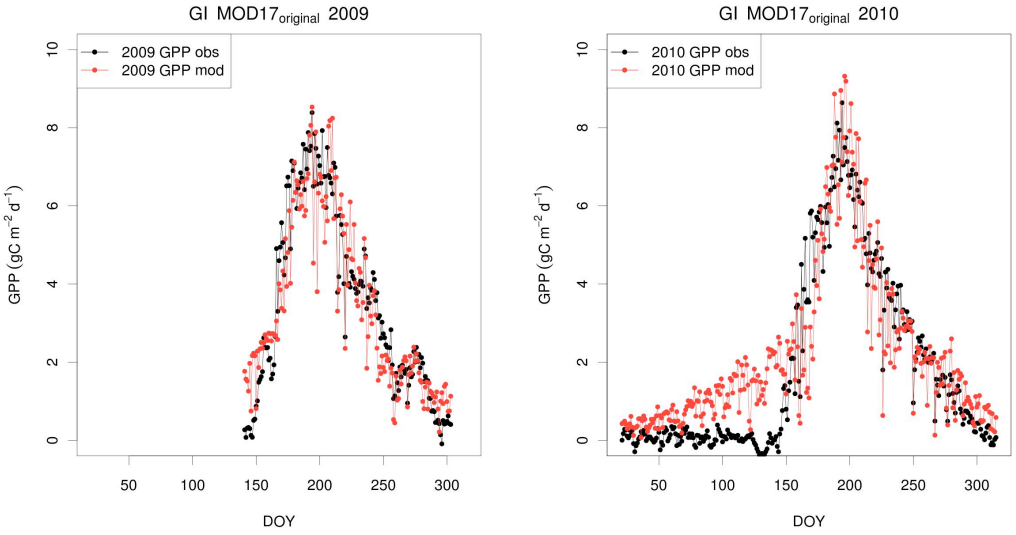

Figure 4.17: *$MOD17_{original}$ 2009 (left) and 2010 (right) results. Seasonal dynamics of measured (black) and modelled (red) GPP in 2009 and in 2010 are showed. Model parameters were optimised in 2009 and the performance of the parametrization was tested using the 2010 data.*

The use of the formulation that considers the snow threshold ($MOD17_{snow}$, figure 4.18) overcame the problem of early season overestimation, and gave better results in 2010 (RMSE= 0.887 $gCm^{-2}d^{-1}$, EF=0.854, r^2=0.868).

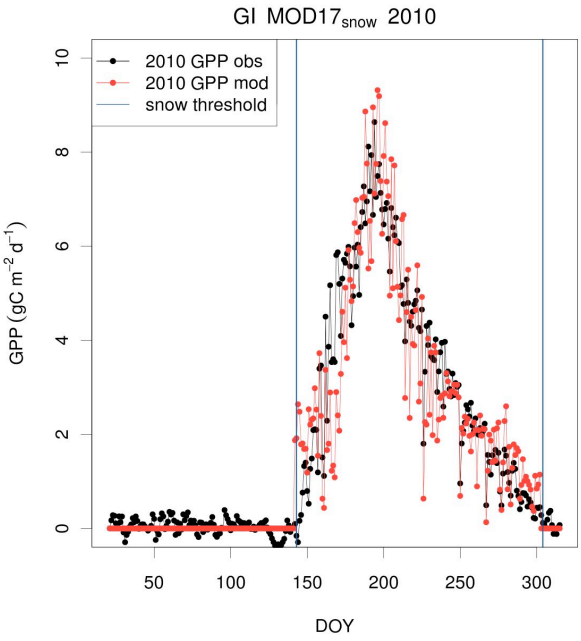

Figure 4.18: *$MOD17_{snow}$ simulation: seasonal dynamics of measured (black) and modelled (red) GPP in 2010 are showed. Vertical lines indicate DOY of snow-melt and snow-in.*

The formulation MOD17$_{Ts}$ (figure 4.19), generally gave better results both in 2009 and 2010 simulation estimates (RMSE= 0.833 and 0.864 gCm^{-2}d^{-1} , EF=0.876 and 0.863, r^2=0.887 and 0.879). In particular this formulation allowed a good estimate of the timing of GPP rise in 2010 without the need of a snow threshold. MOD17$_{Ts}$ provided the best estimates of cumulative GPP, highly in accordance with the observed cumulative both in 2009 (observed GPP=565.0 gCm^{-2}, modeled GPP = 565.6 gCm^{-2}) and 2010 (observed GPP=537.4 gCm^{-2}, modeled GPP = 538.0 gCm^{-2}).

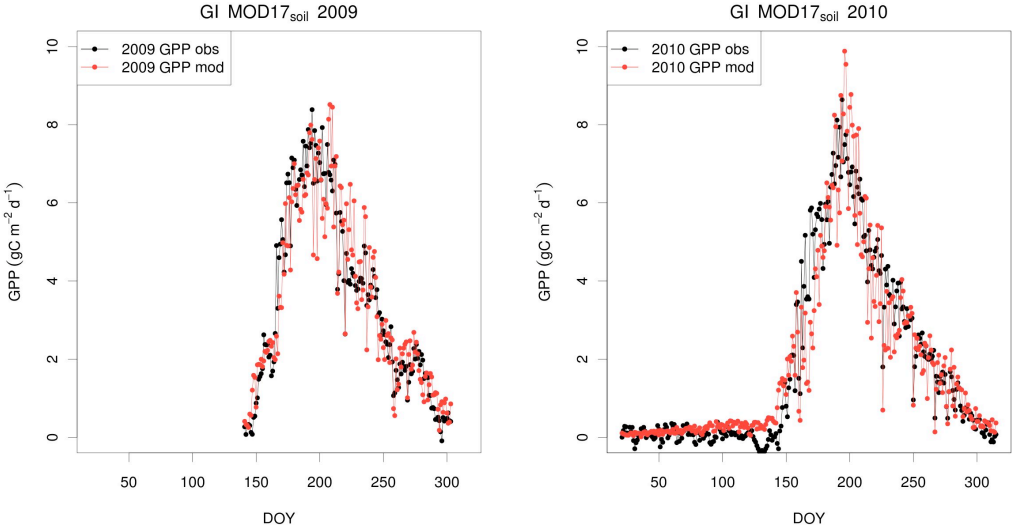

Figure 4.19: *MOD17$_{Ts}$ 2009 (left) and 2010 (right) results. Seasonal dynamics of measured (black) and modelled (red) GPP in 2009 and in 2010 are showed. Model parameters were optimised in 2009 and the performance of the parametrization was tested using the 2010 data.*

MOD17$_{SWC}$ (figure 4.20) that included SWC in place of VPD gave good results, but however did not differed substantially from those of MOD17$_{original}$ and, since it was associated with Ta, it required a snow threshold as well. On the other hand, MOD17$_{Ts,SWC}$, showed in figure 4.21, joined the advantages of the use of soil temperature with the use of SWC and provided better estimates (RMSE= 0.990 gCm^{-2}d^{-1}, EF=0.824, r^2=0.841 in 2009 and RMSE=0.88 gCm^{-2}d^{-1}, EF=0.857, r^2=0.873 in 2010).

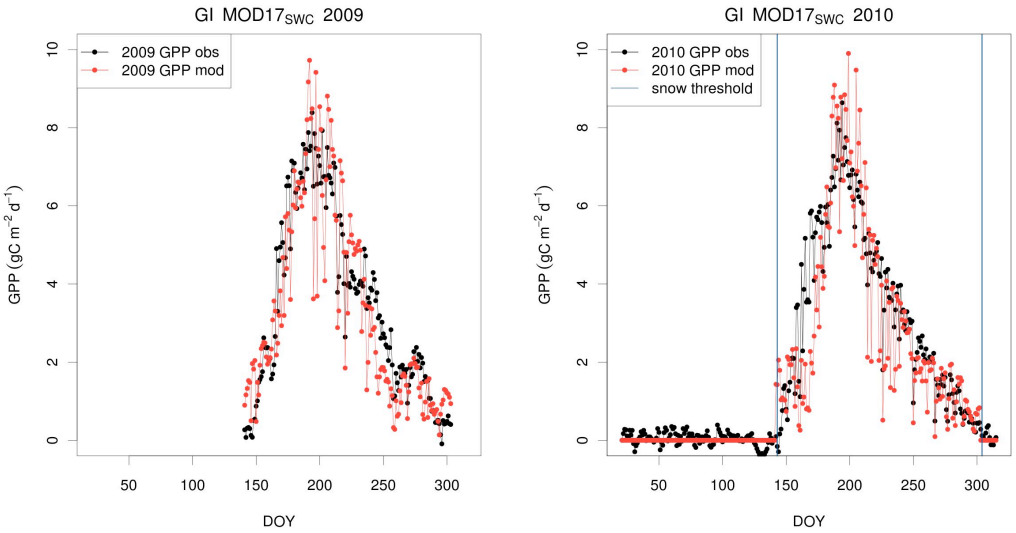

Figure 4.20: *MOD17$_{SWC}$ 2009 (left) and 2010 (right) results. Seasonal dynamics of measured (black) and modelled (red) GPP in 2009 and in 2010 are showed. A snow threshold is applied in 2010. Model parameters were optimised in 2009 and the performance of the parametrization was tested using the 2010 data.*

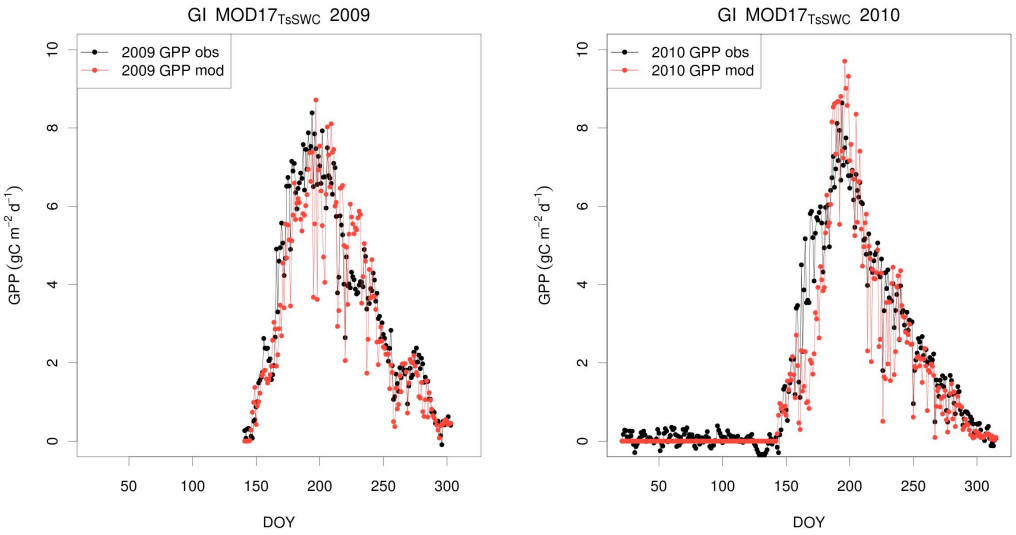

Figure 4.21: *MOD17$_{Ts,SWC}$ 2009 (left) and 2010 (right) results. Seasonal dynamics of measured (black) and modelled (red) GPP in 2009 and in 2010 are showed. Model parameters were optimised in 2009 and the performance of the parametrization was tested using the 2010 data.*

	Model formulation	2009 RMSE ($gCm^{-2}d^{-1}$)	2009 EF	2009 r^2	2010 RMSE ($gCm^{-2}d^{-1}$)	2010 EF	2010 r^2
	$MOD17_{original}$	0.981	0.828	0.829	1.029	0.790	0.816
	$MOD17_{snow}$				0.887	0.854	0.868
GI	$MOD17_{Ts}$	0.833	0.876	0.887	0.864	0.863	0.879
	$MOD17_{SWC}$	1.092	0.795	0.813	0.936	0.835	0.852
	$MOD17_{Ts,SWC}$	0.990	0.824	0.841	0.880	0.857	0.873

Table 4.5: *Summary of fitting statistics (Root Mean Square Error, RMSE, model efficiency, EF and determination coefficient, r^2) of different model formulations used to simulate daily GPP. Digital camera Greenness Index (GI) was used as a proxy of fAPAR in combination with different meteorological drivers: Ta_{Min} and VPD, without ($MOD17_{original}$) and with a snow threshold ($MOD17_{snow}$),Ts_{Min} and VPD ($MOD17_{Ts}$), Ta_{Min} and SWC ($MOD17_{SWC}$), Ts_{Min} and SWC ($MOD17_{Ts,SWC}$).*

4.5.1 Parameter uncertainty evaluation

In this section results of the analysis on parameter uncertainty are presented. As an example results obtained with the original formulation of MOD17 constrained by the snow threshold (i.e, $MOD17_{snow}$) driven by webcam GI are showed. Following the method described in section 3.4.4, 60 parameter sets (over 300 tested) considered "as good as" the best set of model parameters estimated were use to run the model forward with the aim of propagate the uncertainty of model parameters into GPP estimates. The uncertainty in modelled GPP due to model parameters uncertainty is represented in figure 4.22: the seasonal course of daily GPP in 2009 and 2010 obtained using the best-fit model parameters is represented in red, while grey area represents the 90% CI of the modeled daily GPP.

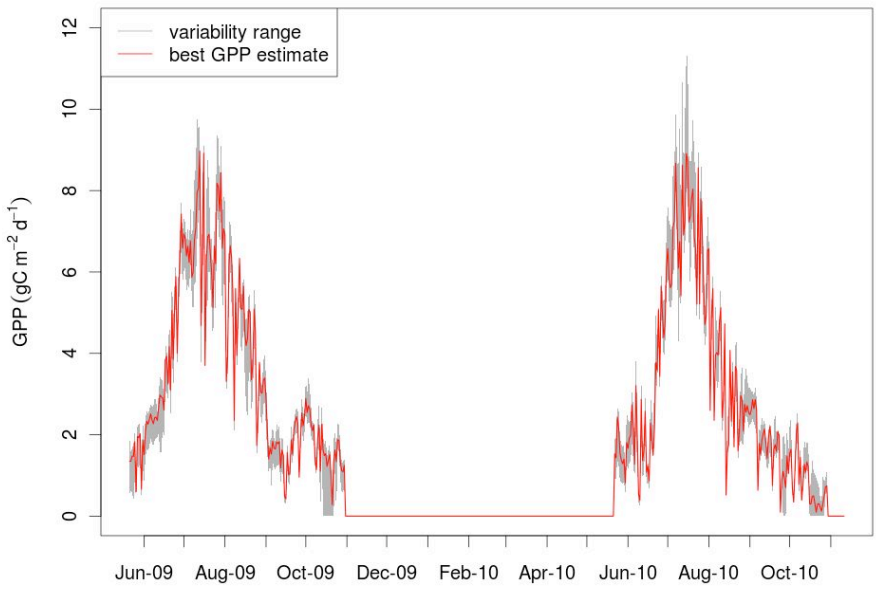

Figure 4.22: *Course of daily 2009 and 2010 GPP obtained using the best model fit parameters of $MOD17_{snow}$ driven by webcam GI (red line) and GPP estimates range due to parameter uncertainty (grey area)*

The results obtained from this analysis is referred only to one source of uncertainty (i.e. model parameter uncertainty) and showed that model parameters can be constrained quite well using MOD17 driven by meteorology and using GI as proxy

of the fAPAR. The magnitude of the uncertainty related to model parameters was similar across model structures (data not shown).

4.5.2 Comparing GI, NDVI and MTCI

We compared the use of GI in simulating GPP daily variability with the use of spectral indices computed from HSI data. In figure 4.23 results of $MOD17_{original}$ driven by NDVI is presented. The use of NDVI gave slightly worse results (table 4.6) compared to the use of GI, both in optimisation 2009 (RMSE= 1.133 $gCm^{-2}d^{-1}$, EF=0.724, r^2=0.734) and in the evaluation of 2010 simulation (RMSE= 1.103 $gCm^{-2}d^{-1}$, EF=0.71, r^2=0.73). Looking at the seasonal course of modelled GPP it can be seen that NDVI failed in describing the decreasing phase of late summer-autumn. On the contrary, the use of MTCI (figure 4.24) provided good estimates in both years (table 4.6). This is due to the fact that NDVI is less sensitive to little green variations compared to GI and MTCI and it is by far more related to structure, LAI and total biomass, while MTCI is based on wavelengths in the red-edge region which is more sensitive to chlorophyll and green variations (*Dash and Curran*, 2004).

Model formulation		2009			2010		
		RMSE ($gCm^{-2}d^{-1}$)	EF	r^2	RMSE ($gCm^{-2}d^{-1}$)	EF	r^2
NDVI	$MOD17_{original}$	1.133	0.724	0.734	1.103	0.710	0.730
MTCI	$MOD17_{original}$	0.896	0.827	0.843	0.970	0.834	0.761

Table 4.6: *Summary of fitting statistics (Root Mean Square Error, RMSE, model efficiency, EF and determination coefficient, r^2) $MOD17_{original}$ using NDVI (Normalized Difference Vegetation Index) and MTCI (MERIS Terrestrial Chlorophyll Index) as proxy of fAPAR.*

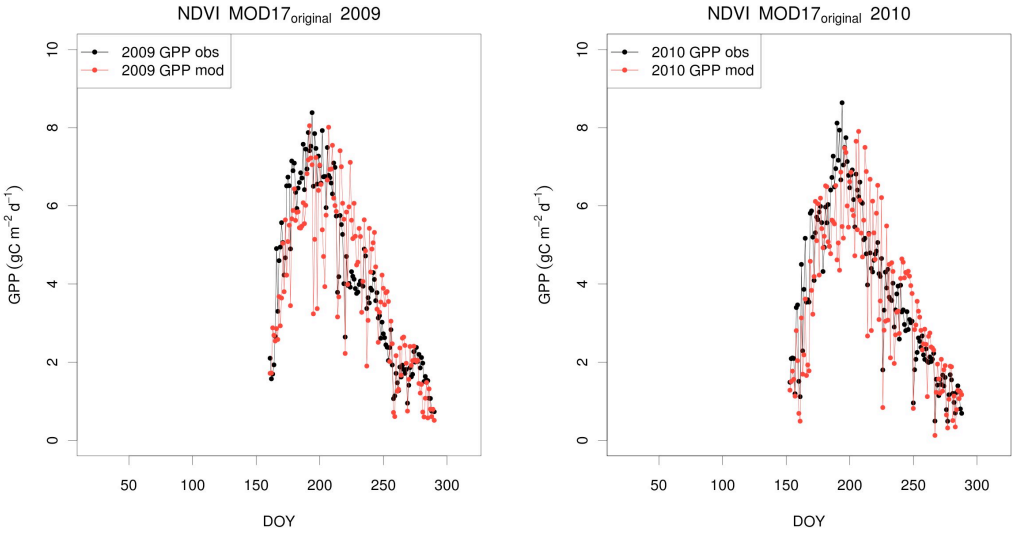

Figure 4.23: *$MOD17_{NDVI}$ 2009 (left) and 2010 (right) results. Seasonal dynamics of measured (black) and modelled (red) GPP in 2009 and in 2010 are showed. Model parameters were optimised in 2009 and the performance of the parametrization was tested using the 2010 data.*

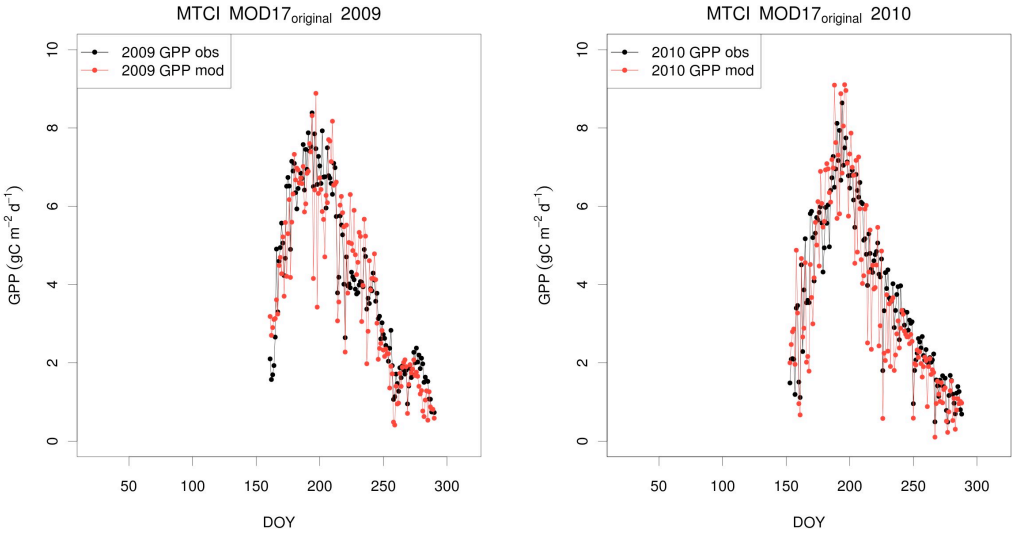

Figure 4.24: *$MOD17_{MTCI}$ 2009 (left) and 2010 (right) results. Seasonal dynamics of measured (black) and modelled (red) GPP in 2009 and in 2010 are showed. Model parameters were optimised in 2009 and the performance of the parametrization was tested using the 2010 data.*

5 DISCUSSION

The aim of this research was to study the CO_2 exchange of a mountain grassland using eddy covariance method integrated with proximal sensing observations and application of LUE models.

The studied grassland is an important site for CO_2 exchange researches, mainly because it is a poorly investigated ecosystem in carbon cycle studies, located in a remote area, at high elevation (2160 m asl) and characterised by a long duration of the snow season. Moreover the fast dynamics of carbon fluxes and canopy greening, and the typical alpine climate, represent an interesting test-case for developing primary production models.

Eddy covariance was used to continuously measure the CO_2 Net Ecosystem Exchange (NEE) and derive its major component processes, Gross Primary Production (GPP) and ecosystem Respiration (Reco) at half-hourly time step, allowing the analysis of carbon flux dynamics at different time scales. Given theoretical assumptions (flat terrain, fully turbulent flux, uniform target vegetation, negligible air density fluctuations and flow divergence) required for the application of the method, and the general complexity of the application of such measurements in mountain environments (*Hammerle et al.*, 2007; *Hiller et al.*, 2008), eddy covariance measurements need an accurate evaluation of the data quality. We found that during the study period (from June 2008 to December 2010) the data quality, evaluated on the basis of well established standard procedures (*Wilson et al.*, 2002; *Mauder and Foken*, 2004), fell within the range published in recent literature (*Marcolla and Cescatti*, 2005; *Wohlfahrt et al.*, 2008b). In detail, we found that more data were rejected during the winter period, while data coverage during the growing season was in the average reported by other studies (*Xu and Baldocchi*, 2004; *Rogiers et al.*, 2005;

Wohlfahrt et al., 2008b).

Regarding energy balance closure, the greatest imbalance occurred during winter period. This can be explained by the definition of energy balance, formulated in terms of energy exchanges taking place within an interface that is assumed infinitesimally thin and having neither mass nor specific heat exchanges. Penetration of shortwave radiation into the snowpack as well as mass movements and phase changes within the snowpack make this concept barely applicable to a snow covered surface (*Armstrong and Brun*, 2008). During the season of vegetation activity, energy balance closure assessed with two different methods (linear regression (slope) and EBR) supported the consistency of flux measurements. In detail, since the energy storage (e.g. biomass and soil energy storage), one of the component of the energy balance, was not considered, the method based on linear regression between half-hourly data of turbulent fluxes (H and LE) and available energy (Rn - G), could be affected by small scale changes in energy storage. Compared to linear regression, EBR (described in section 3.3.2.2) gave indication of an higher seasonal energy balance closure. Even if EBR was thought to potentially overlook biases in the half-hourly data, (*Wilson et al.*, 2002) (such as underestimated fluxes at night), using this method energy storage tend to be null by summation of energy balance terms over a wider time period. As a consequence, comparison of results from the two methods demonstrated that a certain percentage of summer imbalance could be explained by neglected energy storage rather than inaccurate eddy covariance measurements.

Finally the evaluation of the distribution of X_{max} and of the wind field confirmed that during the growing season the measured scalar flux was representative of the study area and that the contribution of fluxes from the target ecosystem is by far dominating the overall budget.

Proximal sensing in this study was mainly oriented towards the use of a digital camera that continuously tracked the phenology of the vegetation and the extraction of a colour index (Greenness Index, GI) related to canopy greenness. Results showed that digital camera imagery is well-suited for monitoring phenology (in terms of canopy greenness) of a mountain grassland. The greenness index derived from collected images provided reliable information on vegetation status with a

daily temporal resolution. This achievement offered the possibility of a continuous monitoring of timing and rate of grass development that is not feasible with traditional phenological observations in such ecosystems, often located in remote areas. The experience of PhenoALP project, which provided major information on the monitoring of grassland phenology and defined a field protocol for plant phenology, outlined indeed the complexity to obtain an integrated indicator of canopy development with traditional field observations, because of the high biodiversity of (alpine) grassland (*Körner*, 2003).

Moreover the comparison of well-known spectral indices (NDVI and MTCI) derived from an Hyperpectral Irradiometer (HSI) (*Meroni et al.*, 2011; *Cogliati*, 2011) with the colour index (i.e. GI) derived from digital photography further demonstrated the reliability of the use of GI in following changes in canopy structure and in LUE models aimed at the description of GPP.

In the following sections results derived from the integration of the described approaches are discussed.

Analysis of carbon fluxes and Vegetation Indices variations

Through the analysis of NEE, GPP, Reco, GI and meteorology time-courses over the study period, the carbon flux dynamics and the vegetation development of this mountain ecosystem were characterised. The study site, located at an elevation of 2160 m slm, undergoes a strong seasonality of the environmental factors that highly influence ecosystem processes. In particular the snow cover duration regulated the short period available for the vegetation development and activity, that lasted approximately 5 months. During the brief growing season carbon fluxes showed a clear seasonal time-course, similar within the three years of study: photosynthesis was optimised trough a fast increase of carbon uptake at the beginning of the growing season until its maximum peak, nearly in the middle of July, while in the second part of the season a slower decline is observed; ecosystem respiration on the contrary showed a fairly constant increasing and decreasing trend. This kind of trend is likely to be similar to other high elevation grassland (*Körner*, 2003) but different from trend found in other cold climate ecosystems (*Humphreys and Lafleur*, 2011).

No particular differences were found in the duration of the growing season assessed by several methods. In particular results confirmed that the photosynthetic activity, considered both as gross and net uptake, started few days after the snow-melt in late spring. On the other hand, in autumn the end of the growing season, especially from a functional point of view, occurred several days (10-15) before the first snow fall. Considering weather conditions, while at the moment of snow disappearance developing grass generally faced to non-limitant conditions, in autumn the decreasing trend of meteorological variables likely had a stronger downregulating effect on photosynthesis. Studies on grassland located at lower elevation (*Wohlfahrt et al.*, 2008b), where snow-melt occurred earlier in the season reported that ecosystem turned to a sink several days (on average 25 days) after snow-melt and during this period the grassland continued to lose carbon on a daily basis.

Different authors underlined (*Körner*, 2003; *Jonas et al.*, 2008) how snow cover is, on the one hand, a physical constraint for vegetation development and functioning, but at the same time it has a protective role for plants from the severe weather stresses typical of cold climate environments. As a consequence, considering Torgnon grassland, the favourable spring weather occurred after snow-melt allowed the fast carbon uptake at the beginning of the growing season.

Despite the observed inter-annual similar trends of carbon fluxes and duration of the growing season, small differences, found in seasonal cumulative NEE, GPP and Reco among years, seemed to be related to the timing of certain meteorological events. No particular differences were indeed found in overall meteorological data within years, except for snow height, SWE and the total amount of summer precipitation in 2009 and 2010. Higher seasonal values of GPP and NEE (and lower Reco) were found in 2009, the year with an higher water (and probably nutrients) input at the beginning of the season and more dry conditions (i.e. lower PPT and SWC) during summer; lower values of carbon uptake (and higher Reco) were found in 2010, the year with a lower snow depth and higher total amount of PPT and SWC in summer. These results gave an indication of the importance of the timing of water availability: water from the snow-melt potentially had a major (or different) role compared to total seasonal precipitation and SWC. Even if in a different ecosystem (high elevation subalpine forest), *Monson et al.* (2002) found that the spring avail-

ability of liquid soil water after snow melt, combined with warmer temperatures, constitutes the set of environmental controls causing full recovery of carbon uptake. In particular *Monson et al.* (2005) stated that, although the use of the melted snow water continues for some time after snow melt, the use of winter snow versus summer rain water is not yet clearly understood and thus it is an interesting issue to deepen. Moreover the autumnal course of NEE in 2009 did not exhibited those peaks of localised changes towards a net release, occurring in other years. This fact was related to particular favourable events (soil temperature and moisture) found in that specific period compared to other years. Another study (*Xu and Baldocchi*, 2004) reported, for a Mediterranean grassland, that the timing of rain events had more impact than the total amount of precipitation on ecosystem GPP and NEE.

As GPP, the time-course of GI during two years of observation confirmed that in this mountain grassland development of the canopy was strongly controlled by snow cover duration and in particular by snow-melt date: once snow disappeared the canopy suddenly started to green-up as outlined also in *Jonas et al.* (2008). These observations have been investigated in *Migliavacca et al.* (2011a), a study aimed at monitoring and modelling vegetation phenology and physiology at Torgnon grassland. With a model data fusion approach combining the Growing Season Index (GSI) (*Jolly et al.*, 2005) and colour indices derived from digital photography (GI), authors found that main environmental cues identified for grasslands phenology were snow-melting in spring, while autumn phenology was the result of the combined effect of cold temperatures and decreasing day length.

Considering BGS dates the lag observed in spring increasing trend between GI and GPP was mainly related to the pattern of canopy green-up: matgrass (*Nardus stricta* L.), which is the dominant graminaceous species at the site, started to green from the bottom, below the dry and brown dead biomass of the previous year, thus not completely perceptible by the camera low view angle. GI tracked the increases in canopy greenness only when green parts started to be more visible from above. The result of this mechanism was a delay of a few days (5-7 days) between GPP and GI in BGS dates.

In 2009, during late summer-autumn, when senescence mechanisms were already active and the canopy was yellowing, a week characterised by favourable weather

conditions resulted in a rebound of GI that followed the stimulation of photosynthetic activity highlighted by the concomitant observed increase in GPP. This autumnal functional and structural recovery, well detected by GPP and GI, was also detected by MTCI but not by NDVI. During senescence inactive phytoelements on the top canopy increased, however, a fraction of green biomass, which maintained photosynthetic activity as revealed by GPP, was still present. In both years autumn NDVI reacted slower than MTCI to variations in chlorophyll content and green biomass due to the fact that NDVI is more related to structure, LAI and total biomass while the MTCI index is based on wavelengths in the red-edge region which is more sensitive to chlorophyll and green variations (*Dash and Curran*, 2004). As GI responses and fluctuations were similar to the ones of more sophisticated VIs such as the MTCI, these observations allowed to highlight the potential usefulness of digital repeat photography in accurately tracking weekly variations in canopy greenness.

Finally EGS dates between GI and GPP differed by 9-13 days: this fact is in part due to noise in GI curve at the end of the growing season.

For the reasons explained (green-up pattern and noise at the end of the GI curve), the comparison between GI and GPP curves could be done considering narrower thresholds (e.g., 75 %, data not shown) both for BGS and EGS. However, if the aim is to track changes in GSL within years, as result of interannual variation in climate, the threshold of 10 % better represents BGS and EGS events.

Multi-scale analysis of environmental controls over carbon exchange

Wavelet coherence analysis allowed to discern controls of different environmental factors on photosynthesis (GPP) at multi-temporal scales, from day to year. Furthermore this analysis clarified some issues emerged from the comparison of carbon flux and meteorological time-series. The main findings of wavelet analysis is that at big time-scale (seasonal and inter-seasonal), GPP was particularly associated with those factors that are influenced by snowpack presence, i.e. soil temperature and moisture, while at lower time-scales, during the growing season, photosynthetic processes depend on daily temperature (both air and soil) and PAR cycles. These results confirmed that the snow cover has an important action in protecting vege-

tation from the outside environment, indeed by thermal insulation snow dampens soil temperature oscillations and generally keep soil far from freezing temperature (*Zhang*, 2005). In detail snow limited the influence of meteorological factors such as PAR and air temperature at seasonal time scale: the increase of temperature and PAR occurs earlier than the date of snow-melt and the grassland, covered by snow, can not be influenced by those factors.

Localised coherences proper of each growing season were found, highlighting how multiple factors influenced photosynthesis differentially within years and in particular period of the season.

Wavelet analysis between GPP and soil temperature revealed a strong coherence at multiple time scales and, compared to air, showed a clear inter-seasonal influence. A localised coherence of several days just after the snow-melt, outlined the role that the fast rise showed by soil temperature has in driving the concurrent fast rise described for GPP in spring. Soil temperature kept above zero and stable below the insulating snow pack, suddenly raised to high values after the snow melt thus providing good condition for photosynthetic activity.

The role of soil temperature on photosynthetic activity is outlined also by a weekly coherence evident at the end of growing season 2009 during which the recovery of GPP occurred.

As soil temperature, SWC showed an important coherence at inter-seasonal scale, and a weak coherence just after the snow-melt in 2009, not present in 2010. Considering that 2009 and 2010 are contrasting years regarding the amount of winter snow depth and SWC in early spring, this coherence could underline the role of snow water storage on subsequent GPP raise. As previously described, other authors *Körner* (2003); *Monson et al.* (2002, 2005) remarked the role of available liquid water on spring carbon uptake recovery. Beside, also the availability of nutrients is a critical factor at the beginning of the growing season. Nevertheless the role of the amount of nutrients stored in the snowpack and their release at snow melt is not well clarified (*Kuhn et al.*, 1998) and could be an interesting point of development.

Weekly coherences between SWC and GPP were observed along all the study period revealing the delayed effect of rain pulses on photosynthetic activity that lasted for several days (2-8 days). These pulses especially when associated with

warm temperature are known to highly influence the respiration component in other ecosystems (*Vargas et al.*, 2011), thus resulting in lower NEE. The latter represents another interesting issue to investigate in the studied grassland.

Wavelet analysis between PAR and GPP, clearly showed the expected daily coherence between incident photosynthetically active radiation and photosynthesis, while at the end of growing season 2010 low values of PAR were in coherence with the decreasing phase of GPP.

In summary, the wavelet coherence analysis allowed to *i)* distinguish the timescale of influence of diverse meteorological factors over GPP in this grassland; *ii)* draw insights on the (small) differences observed in GPP among years on the basis of localised events, such as an higher input of water at the beginning of 2009, some days of particular warmer soil temperature at the end of 2009, and some days of particular unfavourable PAR condition at the end of 2010.

Gross Primary Production modelling

The analysis based on LUE models highlighted that GPP can be efficiently modelled by combining a color index (GI), derived from the analysis of digital camera images, with different meteorological drivers. The approach was based on the algorithm MOD17 (*Heinsch et al.*, 2006) that considers as meteorological limiting factors, air temperature and VPD. Since, in this mountain ecosystem other meteorological factors, such as snow, soil temperature and SWC, emerged to exert an important role, we tested different model formulations considering those factors.

In detail, results demonstrated that the use of the original MOD17 formulation in this ecosystem, highly influenced by the presence of snow on ground, caused an overestimation in simulating GPP at the beginning of the season. As previously described, the physical separation of ground vegetation from the factors considered in the original model formulation caused a divergence in estimated and measured early season data. The same problem is not evident at the end of the growing season because vegetation activity declined before the first snow fall. As observed from the seasonal courses of carbon components and meteorological factors, the day of snow-melt had a greater influence on CO_2 fluxes compared to the date of snow

appearance as, while in spring photosynthetic activity is physically limited by the snowpack, in autumn both photosynthesis and phenology were mainly influenced by the combined effect of declining meteorological factors. With original MOD17 formulation temporal variability of daily GPP during the growing season is generally well represented, hence the application of a simple snow presence/absence threshold overcame the problem of spring overestimation. However the application of this kind of threshold does not give further insights on the actual functioning of the ecosystem in this particular period of the season. The use of soil temperature rather than air temperature allowed to correctly estimate GPP rise at the beginning of the season even without the use of the snow threshold. This result confirmed the higher coupling between photosynthesis and soil temperature compared to air temperature and indicates that in this grassland soil temperature can be a better predictor of GPP dynamics, rather than air temperature, at least at the beginning of the growing season.

The model that consider the use of SWC rather than VPD when associated with air temperature needed the application of the snow threshold as well. On the contrary, when SWC was associated with soil temperature, model statistics revealed overall better estimates and the GPP estimates were able to reproduce the fast spring increase after snow melt (without the snow threshold).

In this study the role of SWC compared to VPD did not show particular improvements of the results, nevertheless this fact can be in part due the specific linear function used in the model formulation, not completely able to well represent SWC limitation on photosynthesis. The use of other functions (e.g. logistic) could improve the description of SWC constraints and thus GPP estimates (*Veroustraete et al.*, 2002; *Richardson et al.*, 2007a).

The results obtained from the analysis of model parameter uncertainty indicated that model parameters can be constrained quite well using MOD17 driven by meteorology and using GI as proxy of the fAPAR. However, this analysis did not explore the other sources of uncertainty necessary to describe the overall uncertainty in GPP estimates such as the model structure uncertainty (i.e. test different model formulations) and the forcing driver uncertainty, that in this case can be considered almost negligible since the meteorological driver were measured 3.2.2.

The comparison between models driven by GI with those driven by well known spectral indices, such as NDVI and MTCI, gave interesting information on the reliability of the use of GI in LUE models. In particular, the use of NDVI resulted in slight worse estimated, since this index is particularly related to canopy structure and total biomass; while result of GI are more similar to those obtained with the MTCI, closely related to green biomass which controls the energy absorbed by photosynthetic pigments and thus effectively used for photosynthetic processes.

In order to provide more robust GI times series, further work is required to overcome problems related to the image quality issue and data filtering. In fact, while digital camera imagery are very useful for monitoring the seasonal development of the canopy greenness, uncertainty still exists concerning the use of color indices for monitoring the interannual variability of canopy structural parameters and future efforts should be focused to address this issue (*Migliavacca et al.*, 2011a).

Considering a distributed application of models driven by phenology in similar ecosystem (e.g. trough webcam network), even if our results highlighted the better results are obtained using soil temperature which are data not frequently available, its feasibility is not precluded: model formulation based on air temperature and VPD have been demonstrated to be able to well capture overall GPP dynamics when associated to a snow threshold that can be easily obtained, when a snow depth measure is not available, from webcam images or remotely sensed data.

CONCLUSION

The present study used the eddy covariance method to measure carbon dioxide exchange of an unmanaged subalpine grassland, a poorly investigated ecosystem, from June 2008 to the end of 2010. Eddy covariance measurements were integrated with proximal sensing observations in order to follow the phenology, i.e. the structural development, of the canopy in a continuous and automated way. This study showed that a digital camera (a relatively low-cost tool) can provide reliable information for monitoring canopy development and functioning of subalpine grasslands.

With eddy covariance measurements and a color index (GI) derived from digital images, we characterised the duration of the growing season and the dynamics of carbon fluxes and canopy greenness. We derived several insights on the role of snow-cover duration and date of snow-melt on the subsequent canopy development and functioning.

Considered that several controlling factors may act on carbon uptake processes in a non-stationary way and at multiple temporal scales (*Baldocchi et al.*, 2001b; *Vargas et al.*, 2011), a spectral approach was used to analyse these relations: wavelet coherence analysis outlined the periodicities at which different meteorological factors may control GPP in this grassland. A particularly strong coherence was found between soil temperature and GPP at several time-scale which indirectly demonstrate also the influence of the long duration of snowpack in this ecosystem.

This work showed that combining information derived by greenness index (GI) extracted from a digital camera and meteorological factors in light use efficiency model it is possible to well describe the temporal variability of Gross Primary Production (GPP).

At Torgnon, measurements were made throughout the whole year, hence, more year-data, associated to a deeper evaluation of wintertime fluxes (for example by comparison with the CO_2 gradient method through the snow pack (*Liptzin et al.*, 2009)) will allow an assessment of the sink/source strength of an ecosystem for which this information is still lacking.

As other works have previously suggested (*Körner*, 2003; *Jonas et al.*, 2008) all method applied agree in confirming that snow is a major controlling factor in this kind of ecosystem with a direct influence in determining the beginning of the grow-

ing season, but also indirectly by limiting the potential influence of other factors both on carbon uptake and phenology in spring. This study could contribute to recent researches in the field area of carbon cycle that aim at evaluating the effects of future climate change on diverse terrestrial ecosystems. Nevertheless more years of measurements are required to understand how this subalpine grassland could respond to differences in snow-melt dates and how carbon uptake could be affected by earlier snow-melt and/or changes in water and nutrients supply in spring.

References

Armstrong, R., and E. Brun (2008), *Snow and climate: physical processes, surface energy exchange and modeling*, Edited by RL Armstrong and E. Brun. Cambridge: Cambridge University Press, 2008.

Aubinet, M., A. Grelle, A. Ibrom, U. Rannik, J. Moncrieff, et al. (2000), Estimates of the annual net carbon and water exchange of forests: the EUROFLUX methodology, *Advances in Ecological Research*, *30*, 113–175.

Aubinet, M., B. Chermanne, M. Vandenhaute, B. Longdoz, M. Yernaux, and E. Laitat (2001), Long term carbon dioxide exchange above a mixed forest in the Belgian Ardennes, *Agricultural and Forest Meteorology*, *108*(4), 293–315.

Bahn, M., M. Rodeghiero, M. Anderson-Dunn, S. Dore, C. Gimeno, M. Drosler, M. Williams, C. Ammann, F. Berninger, C. Flechard, et al. (2008), Soil respiration in European grasslands in relation to climate and assimilate supply, *Ecosystems*, *11*(8), 1352–1367.

Baldocchi, D. (2008), Breathing'of the terrestrial biosphere: lessons learned from a global network of carbon dioxide flux measurement systems, *Australian Journal of Botany*, *56*(1), 1.

Baldocchi, D., and K. Wilson (2001), Modeling CO_2 and water vapor exchange of a temperate broadleaved forest across hourly to decadal time scales, *Ecological Modelling*, *142*(1-2), 155–184.

Baldocchi, D., B. Hincks, and T. Meyers (1988), Measuring biosphere-atmosphere exchanges of biologically related gases with micrometeorological methods, *Ecology*, *69*(5), 1331–1340.

Baldocchi, D., E. Falge, L. Gu, R. Olson, D. Hollinger, S. Running, P. Anthoni, C. Bernhofer, K. Davis, and R. Evans (2001a), FLUXNET: A new tool to study the temporal and spatial variability of ecosystem-scale carbon dioxide, water vapor, and energy flux densities., *Bulletin of the American Meteorological Society*, *82*(11), 2415–2434.

Baldocchi, D., E. Falge, and K. Wilson (2001b), A spectral analysis of biosphere-atmosphere trace gas flux densities and meteorological variables across hour to multi-year time scales, *Agricultural and Forest Meteorology*, *107*(1), 1–27.

Baldocchi, D., T. Black, P. Curtis, E. Falge, J. Fuentes, A. Granier, L. Gu, A. Knohl, K. Pilegaard, H. Schmid, et al. (2005), Predicting the onset of net carbon uptake by deciduous forests with soil temperature and climate data: a synthesis of FLUXNET data, *International Journal of Biometeorology*, *49*(6), 377–387.

Baldocchi, D. D. (2003), Assessing ecosystem carbon balance: problems and prospects of the eddy covariance technique, *Global Change Biology*, *9*, 479–4..

Bradley, B., R. Jacob, J. Hermance, and J. Mustard (2007), A curve fitting procedure to derive inter-annual phenologies from time series of noisy satellite NDVI data, *Remote Sensing of Environment*, *106*(2), 137–145.

Burba, G. G., and D. J. Anderson (2010), *A Brief Practical Guide to Eddy Covariance Flux Measurements. Principles and Workflow Examples for Scientific and Industrial Applications*, LI-COR Biosciences, Lincoln, USA.

Cao, M., and F. Woodward (1998), Dynamic responses of terrestrial ecosystem carbon cycling to global climate change, *Nature*, *393*(6682), 249–252.

Cernusca, A., M. Bahn, F. Berninger, U. Tappeiner, and G. Wohlfahrt (2008), Effects of land-use changes on sources, sinks and fluxes of carbon in European mountain grasslands, *Ecosystems*, *11*(8), 1335–1337.

Chapin, F., P. Matson, and H. Mooney (2002), *Principles of terrestrial ecosystem ecology*, Springer Verlag.

Chen, J., X. Li, T. Nilson, and A. Strahler (2000), Recent advances in geometrical optical modelling and its applications, *Remote Sensing Reviews*, *18*(2), 227–262.

Cogliati, S. (2011), Development of automatic spectrometric systems for proximal sensing of photosynthetic activity of vegetation, Ph.D. thesis, University of Milano Bicocca, Italy.

Collatz, G., J. Ball, C. Grivet, and J. Berry (1991), Physiological and environmental regulation of stomatal conductance, photosynthesis and transpiration: a model that includes a laminar boundary layer, *Agricultural and Forest Meteorology*, *54*(2-4), 107–136.

Cox, P., C. Huntingford, and R. Harding (1998), A canopy conductance and photosynthesis model for use in a GMC land surface scheme, *Journal of Hydrology*, *212*, 79–94.

Dash, J., and P. Curran (2004), The MERIS terrestrial chlorophyll index, *International Journal of Remote Sensing*, *25*(23), 5403–5413.

Falge, E., D. Baldocchi, R. Olson, P. Anthoni, M. Aubinet, C. Bernhofer, G. Burba, R. Ceulemans, R. Clement, H. Dolman, et al. (2001), Gap filling strategies for defensible annual sums of net ecosystem exchange, *Agricultural and Forest Meteorology*, *107*(1), 43–69.

Flanagan, L., L. Wever, and P. Carlson (2002), Seasonal and interannual variation in carbon dioxide exchange and carbon balance in a northern temperate grassland, *Global Change Biology*, *8*(7), 599–615.

Foken, T. (2008), *Micrometeorology*, Springer Verlag.

Foken, T., and B. Wichura (1996), Tools for quality assessment of surface-based flux measurements, *Agricultural and Forest Meteorology*, *78*(1-2), 83–105.

Gash, J., and A. Culf (1996), Applying a linear detrend to eddy correlation data in realtime, *Boundary-Layer Meteorology*, *79*(3), 301–306.

Goulden, M., J. Munger, S. Fan, B. Daube, and S. Wofsy (1996), Measurements of carbon sequestration by long-term eddy covariance: methods and a critical evaluation of accuracy, *Global Change Biology*, *2*(3), 169–182.

Grinsted, A., J. Moore, and S. Jevrejeva (2004), Application of the cross wavelet transform and wavelet coherence to geophysical time series, *Nonlinear Processes in Geophysics*, *11*(5/6), 561–566.

Gu, L., E. Falge, T. Boden, D. Baldocchi, T. Black, S. Saleska, T. Suni, S. Verma, T. Vesala, S. Wofsy, and L. Xu (2005), Objective threshold determination for nighttime eddy flux filtering, *Agricultural and Forest Meteorology*, *128*(3-4), 179–197.

Hammerle, A., A. Haslwanter, M. Schmitt, M. Bahn, U. Tappeiner, A. Cernusca, and G. Wohlfahrt (2007), Eddy covariance measurements of carbon dioxide, latent and sensible energy fluxes above a meadow on a mountain slope, *Boundary-Layer Meteorology*, *122*(2), 397–416.

Heimann, M., and M. Reichstein (2008), Terrestrial ecosystem carbon dynamics and climate feedbacks, *Nature*, *451*(7176), 289–292.

Heinsch, F., M. Reeves, P. Votava, S. Kang, C. Milesi, M. Zhao, J. Glassy, W. Jolly, R. Loehman, C. Bowker, J. Kimball, R. Nemani, and S. Running (2003), Users guide: GPP and NPP (MOD17A2/A3) products, *NASA MODIS land algorithm, version*, *2*.

Heinsch, F., M. Zhao, S. Running, J. Kimball, R. Nemani, K. Davis, P. Bolstad, B. Cook, A. Desai, D. Ricciuto, et al. (2006), Evaluation of remote sensing based terrestrial productivity from MODIS using regional tower eddy flux network observations, *Geoscience and Remote Sensing, IEEE Transactions on*, *44*(7), 1908–1925.

Hilker, T., N. Coops, F. Hall, T. Black, M. Wulder, Z. Nesic, and P. Krishnan (2008), Separating physiologically and directionally induced changes in PRI using BRDF models, *Remote Sensing of Environment*, *112*(6), 2777–2788.

Hiller, R. (2007), Growing season CO_2 budget of an alpine grassland in the swiss alps, Master's thesis, Universitat Bern, Fakultat, Philosophisch naturwissenschaftlichen.

Hiller, R., M. Zeeman, and W. Eugster (2008), Eddy-covariance flux measurements in the complex terrain of an alpine valley in Switzerland, *Boundary-Layer Meteorology*, *127*(3), 449–467.

Horn, J., and K. Schulz (2011), Identification of a general light use efficiency model for gross primary production, *Biogeosciences*, *8*, 999–1021.

Humphreys, E., and P. Lafleur (2011), Does earlier snowmelt lead to greater CO_2 sequestration in two low arctic tundra ecosystems?, *Geophysical Research Letters*, *38*(9), L09,703.

Jolly, W., R. Nemani, and S. Running (2005), A generalized, bioclimatic index to predict foliar phenology in response to climate, *Global Change Biology*, *11*(4), 619–632.

Jonas, T., C. Rixen, M. Sturm, and V. Stoeckli (2008), How alpine plant growth is linked to snow cover and climate variability, *Journal of Geophysical research*, *113*(G3), G03,013.

Kaimal, J., and J. Finnigan (1994), *Atmospheric boundary layer flows: their structure and measurement*, Oxford University Press, USA.

Körner, C. (2003), *Alpine plant life: functional plant ecology of high mountain ecosystems*, Springer.

Kuhn, M., J. Haslhofer, U. Nickus, and H. Schellander (1998), Seasonal development of ion concentration in a high alpine snow pack, *Atmospheric Environment*, *32*(23), 4041–4051.

Lasslop, G., M. Reichstein, D. Papale, A. Richardson, A. Arneth, A. Barr, P. Stoy, and G. Wohlfahrt (2010), Separation of net ecosystem exchange into assimilation and respiration using a light response curve approach: critical issues and global evaluation, *Global Change Biology*, *16*(1), 187–208.

Lieth, H. (1974), *Phenology and seasonality modelling*, Springer, Heidelberg.

Liptzin, D., M. Williams, D. Helmig, B. Seok, G. Filippa, K. Chowanski, and J. Hueber (2009), Process-level controls on CO_2 fluxes from a seasonally snow-covered subalpine meadow soil, Niwot Ridge, Colorado, *Biogeochemistry*, *95*(1), 151–166.

Lloyd, J., and J. Taylor (1994), On the temperature dependence of soil respiration, *Functional Ecology*, *8*(3), 315–323.

Manca, G. (2003), Analisi dei flussi di carbonio di una cronosequenza di cerro (Quercus cerris L.) dell'Italia centrale attraverso la tecnica della correlazione turbolenta, Ph.D. thesis, University of Tuscia, Italy.

Marcolla, B., and A. Cescatti (2005), Experimental analysis of flux footprint for varying stability conditions in an alpine meadow, *Agricultural and Forest Meteorology*, *135*(1-4), 291–301.

Massman, W., and X. Lee (2002), Eddy covariance flux corrections and uncertainties in long-term studies of carbon and energy exchanges, *Agricultural and Forest Meteorology*, *113*(1-4), 121–144.

Mauder, M., and T. Foken (2004), *Documentation and instruction manual of the eddy covariance software package TK2*, Univ., Abt. Mikrometeorologie.

McMillen, R. (1988), An eddy correlation technique with extended applicability to non-simple terrain, *Boundary-Layer Meteorology*, *43*(3), 231–245.

Menzel, A., T. Sparks, N. Estrella, E. Koch, A. Aasa, R. Ahas, K. Alm Kubler, P. Bissolli, O. BraslavskÁ, A. Briede, et al. (2006), European phenological response to climate change matches the warming pattern, *Global Change Biology*, *12*(10), 1969–1976.

Mercalli, L., D. Cat Berro, S. Montuschi, C. Castellano, M. Ratti, G. Di Napoli, G. Mortara, and N. Guindani (2003), *Atlante Climatico della Valle d'Aosta*, Società Meteorologica Subalpina, Torino.

Meroni, M., A. Barducci, S. Cogliati, F. Castagnoli, M. Rossini, L. Busetto, M. Migliavacca, E. Cremonese, M. Galvagno, R. Colombo, et al. (2011), The hyperspectral irradiometer, a new instrument for long-term and unattended field spectroscopy measurements, *Review of Scientific Instruments*, *82*, 043,106.

Migliavacca, M., M. Galvagno, E. Cremonese, M. Rossini, M. Meroni, O. Sonnentag, S. Cogliati, G. Manca, F. Diotri, L. Busetto, A. Cescatti, R. Colombo, F. Fava, U. Morra di Cella, E. Pari, C. Siniscalco, and A. Richardson (2011a), Using digital repeat photography and eddy covariance data to model grassland phenology and photosynthetic CO_2 uptake, *Agricultural and Forest Meteorology, in press*.

Migliavacca, M., et al. (2011b), Semiempirical modeling of abiotic and biotic factors controlling ecosystem respiration across eddy covariance sites, *Global Change Biology*, *17*, 390–409.

Misson, L., D. Baldocchi, T. Black, P. Blanken, Y. Brunet, J. Curiel Yuste, J. Dorsey, M. Falk, A. Granier, M. Irvine, et al. (2007), Partitioning forest carbon fluxes with overstory and understory eddy-covariance measurements: A synthesis based on fluxnet data, *Agricultural and Forest Meteorology*, *144*(1-2), 14–31.

Monson, R., A. Turnipseed, J. Sparks, P. Harley, L. Scott-Denton, K. Sparks, and T. Huxman (2002), Carbon sequestration in a high-elevation, subalpine forest, *Global Change Biology*, *8*(5), 459–478.

Monson, R., J. Sparks, T. Rosenstiel, L. Scott-Denton, T. Huxman, P. Harley, A. Turnipseed, S. Burns, B. Backlund, and J. Hu (2005), Climatic influences on net ecosystem CO_2 exchange during the transition from wintertime carbon source to springtime carbon sink in a high-elevation, subalpine forest, *Oecologia*, *146*(1), 130–147.

Monteith, J. (1972), Solar radiation and productivity in tropical ecosystems, *Journal of Applied Ecology*, *9*(3), 747–766.

Monteith, J., and M. Unsworth (2008), *Principles of environmental physics*, Academic Press.

Nouvellon, Y., D. Seen, S. Rambal, A. Bégué, M. Moran, Y. Kerr, and J. Qi (2000), Time course of radiation use efficiency in a shortgrass ecosystem: Consequences for remotely sensed estimation of primary production, *Remote Sensing of Environment*, *71*(1), 43–55.

Oke, T. (1987), *Boundary layer climates*, Routledge.

Papale, D., M. Reichstein, M. Aubinet, E. Canfora, C. Bernhofer, W. Kutsch, B. Longdoz, S. Rambal, R. Valentini, T. Vesala, et al. (2006), Towards a standardized processing of Net Ecosystem Exchange measured with eddy covariance technique: algorithms and uncertainty estimation, *Biogeosciences*, *3*(4), 571–583.

Piao, S., P. Ciais, P. Friedlingstein, P. Peylin, M. Reichstein, S. Luyssaert, H. Margolis, J. Fang, A. Barr, A. Chen, et al. (2008), Net carbon dioxide losses of northern ecosystems in response to autumn warming, *Nature*, *451*(7174), 49–52.

Porra, R., W. Thompson, and P. Kriedemann (1989), Determination of accurate extinction coefficients and simultaneous equations for assaying chlorophylls a and b extracted with four different solvents: verification of the concentration of chlorophyll standards by atomic absorption spectroscopy, *Biochimica et Biophysica Acta (BBA)-Bioenergetics*, *975*(3), 384–394.

R Development Core Team (2011), *R: A Language and Environment for Statistical Computing*, R Foundation for Statistical Computing, Vienna, Austria, ISBN 3-900051-07-0.

Reichstein, M., E. Falge, D. Baldocchi, D. Papale, M. Aubinet, P. Berbigier, C. Bernhofer, N. Buchmann, T. Gilmanov, A. Granier, et al. (2005), On the separation of net ecosystem exchange into assimilation and ecosystem respiration: review and improved algorithm, *Global Change Biology*, *11*(9), 1424–1439.

Richardson, A., D. Hollinger, J. Aber, S. Ollinger, and B. Braswell (2007a), Environmental variation is directly responsible for short-but not long-term variation in forest-atmosphere carbon exchange, *Global Change Biology*, *13*(4), 788–803.

Richardson, A., J. Jenkins, B. Braswell, D. Hollinger, S. Ollinger, and M. Smith (2007b), Use of digital webcam images to track spring green-up in a deciduous broadleaf forest, *Oecologia*, *152*(2), 323–334.

Richardson, A., B. Braswell, D. Hollinger, J. Jenkins, and S. Ollinger (2009a), Near-surface remote sensing of spatial and temporal variation in canopy phenology, *Ecological Applications*, *19*(6), 1417–1428.

Richardson, A., D. Hollinger, D. Dail, J. Lee, J. Munger, and J. Oḱeefe (2009b), Influence of spring phenology on seasonal and annual carbon balance in two contrasting New England forests, *Tree Physiology*, *29*(3), 321.

Richardson, A., M. Williams, D. Hollinger, D. Moore, D. Dail, E. Davidson, N. Scott, R. Evans, H. Hughes, J. Lee, et al. (2010), Estimating parameters of a forest ecosystem C model with measurements of stocks and fluxes as joint constraints, *Oecologia*, *140*(1), 25–40.

Rogiers, N., W. Eugster, M. Furger, and R. Siegwolf (2005), Effect of land management on ecosystem carbon fluxes at a subalpine grassland site in the Swiss alps, *Theoretical and applied climatology*, *80*(2), 187–203.

Rouse, J., R. Haas, J. Schell, D. Deering, and J. Harlan (1974), Monitoring the vernal advancements and retrogradation of natural vegetation in Nasa, *GSFC, Greenbelt, MD*.

Ruimy, A., P. Jarvis, D. Baldocchi, and B. Saugier (1995), CO_2 fluxes over plant canopies and solar radiation: a review, *Advances in Ecological Research*, *26*, 1–68.

Running, S., and E. Hunt (1993), Generalization of a forest ecosystem process model for other biomes, BIOME-BGC, and an application for global-scale models, *Scaling Physiological Processes: leaf to globe*, pp. 141–158.

Schuepp, P., M. Leclerc, J. MacPherson, and R. Desjardins (1990), Footprint prediction of scalar fluxes from analytical solutions of the diffusion equation, *Boundary-Layer Meteorology*, *50*(1), 355–373.

Sims, D., H. Luo, S. Hastings, W. Oechel, A. Rahman, and J. Gamon (2006), Parallel adjustments in vegetation greenness and ecosystem CO_2 exchange in response to drought in a southern california chaparral ecosystem, *Remote Sensing of Environment*, *103*(3), 289–303.

Solomon, S. (2007), *Climate Change 2007: the physical science basis: contribution of Working Group I to the Fourth Assessment Report of the Intergovernmental Panel on Climate Change*, Cambridge Univ Pr.

Soussana, J., V. Allard, K. Pilegaard, P. Ambus, C. Amman, C. Campbell, E. Ceschia, J. Clifton-Brown, S. Czobel, R. Domingues, et al. (2007), Full accounting of the greenhouse gas (CO_2, N_2O, CH_4) budget of nine European grassland sites, *Agriculture, Ecosystems & Environment*, *121*(1-2), 121–134.

Stoy, P., A. Richardson, D. Baldocchi, G. Katul, J. Stanovick, M. Mahecha, M. Reichstein, M. Detto, B. Law, G. Wohlfahrt, et al. (2009), Biosphere-atmosphere exchange of CO_2 in relation to climate: a cross-biome analysis across multiple time scales, *Biogeosciences*, *6*(10), 2297–2312.

Taiz, L., and E. Zeiger (2010), *Plant Physiology*, Sinauer Associates, Incorporated.

Torrence, C., and G. Compo (1998), A practical guide to wavelet analysis, *Bulletin of the American Meteorological Society*, *79*(1), 61–78.

Valentini, R., G. Matteucci, A. Dolman, E. Schulze, C. Rebmann, E. Moors, A. Granier, P. Gross, N. Jensen, K. Pilegaard, et al. (2000), Respiration as the main determinant of carbon balance in european forests, *Nature*, *404*(6780), 861–865.

Vargas, R., M. Detto, D. Baldocchi, and M. Allen (2010), Multiscale analysis of temporal variability of soil CO_2 production as influenced by weather and vegetation, *Global Change Biology*, *16*(5), 1589–1605.

Vargas, R., M. Carbone, M. Reichstein, and D. Baldocchi (2011), Frontiers and challenges in soil respiration research: from measurements to model-data integration, *Biogeochemistry*, pp. 1–13.

Veroustraete, F., H. Sabbe, and H. Eerens (2002), Estimation of carbon mass fluxes over Europe using the C-Fix model and euroflux data, *Remote Sensing of Environment*, *83*(3), 376–399.

Webb, E., G. Pearman, and R. Leuning (1980), Correction of flux measurements for density effects due to heat and water vapour transfer, *Quarterly Journal of the Royal Meteorological Society*, *106*(447), 85–100.

White, M., K. de Beurs, K. Didan, D. Inouye, A. Richardson, O. Jensen, J. O'Keefe, G. Zhang, R. Nemani, W. van Leeuwen, et al. (2009), Intercomparison, interpretation, and assessment of spring phenology in north america estimated from remote sensing for 1982–2006, *Global Change Biology*, *15*(10), 2335–2359.

White, R., S. Murray, and M. Rohweder (2000), *Pilot analysis of global ecosystems: grassland ecosystems.*, World Resources Institute.

Wilson, K., A. Goldstein, E. Falge, M. Aubinet, D. Baldocchi, P. Berbigier, C. Bernhofer, R. Ceulemans, H. Dolman, C. Field, et al. (2002), Energy balance closure at fluxnet sites, *Agricultural and Forest Meteorology*, *113*(1-4), 223–243.

Wohlfahrt, G., M. Bahn, C. Newesely, S. Sapinsky, U. Tappeiner, and A. Cernusca (2003), Canopy structure versus physiology effects on net photosynthesis of mountain grasslands differing in land use, *Ecological modelling*, *170*(2-3), 407–426.

Wohlfahrt, G., C. Anfang, M. Bahn, A. Haslwanter, C. Newesely, M. Schmitt, M. Drosler, J. Pfadenhauer, and A. Cernusca (2005a), Quantifying nighttime ecosystem respiration of a meadow using eddy covariance, chambers and modelling, *Agricultural and Forest Meteorology*, *128*(3-4), 141–162.

Wohlfahrt, G., M. Bahn, A. Haslwanter, C. Newesely, and A. Cernusca (2005b), Estimation of daytime ecosystem respiration to determine gross primary production of a mountain meadow, *Agricultural and Forest Meteorology*, *130*(1-2), 13–25.

Wohlfahrt, G., M. Anderson-Dunn, M. Bahn, M. Balzarolo, F. Berninger, C. Campbell, A. Carrara, A. Cescatti, T. Christensen, S. Dore, et al. (2008a), Biotic, abi-

otic, and management controls on the net ecosystem CO_2 exchange of European mountain grassland ecosystems, *Ecosystems*, *11*(8), 1338–1351.

Wohlfahrt, G., A. Hammerle, A. Haslwanter, M. Bahn, U. Tappeiner, and A. Cernusca (2008b), Seasonal and inter-annual variability of the net ecosystem CO_2 exchange of a temperate mountain grassland: effects of weather and management, *Journal of Geophysical Research*, *113*(D8), D08,110.

Xiao, X., D. Hollinger, J. Aber, M. Goltz, E. Davidson, Q. Zhang, B. Moore, et al. (2004), Satellite-based modeling of gross primary production in an evergreen needleleaf forest, *Remote Sensing of Environment*, *89*(4), 519–534.

Xu, L., and D. Baldocchi (2004), Seasonal variation in carbon dioxide exchange over a mediterranean annual grassland in california, *Agricultural and Forest Meteorology*, *123*(1-2), 79–96.

Zeeman, M., R. Hiller, A. Gilgen, P. Michna, P. Pluss, N. Buchmann, and W. Eugster (2010), Management and climate impacts on net CO_2 fluxes and carbon budgets of three grasslands along an elevational gradient in Switzerland, *Agricultural and Forest Meteorology*, *150*(4), 519–530.

Zhang, Q., X. Xiao, B. Braswell, E. Linder, F. Baret, and B. Moore III (2005), Estimating light absorption by chlorophyll, leaf and canopy in a deciduous broadleaf forest using modis data and a radiative transfer model, *Remote Sensing of Environment*, *99*(3), 357–371.

Zhang, Q., E. Middleton, H. Margolis, G. Drolet, A. Barr, and T. Black (2009), Can a satellite-derived estimate of the fraction of par absorbed by chlorophyll (faparchl) improve predictions of light-use efficiency and ecosystem photosynthesis for a boreal aspen forest?, *Remote Sensing of Environment*, *113*(4), 880–888.

Zhang, T. (2005), Influence of the seasonal snow cover on the ground thermal regime: An overview, *Reviews of Geophysics*, *43*(4).